Earth-Science Reviews 215 (2021) 103558

Contents lists available at ScienceDirect

Earth-Science Reviews

journal homepage: www.elsevier.com/locate/earscirev

Review Article

Two-stage evolution of glacial-period Asian monsoon circulation by shifts of westerly jet streams and changes of North American ice sheets

Hong Wang [a,b,*], Weijian Zhou [b,d,e], Peixian Shu [b,d,e], Bing Hong [c,d], Zhisheng An [b,d,**]

[a] Interdisciplinary Research Center of Earth Science Frontier, Beijing Normal University, Beijing 100875, China
[b] State Key Laboratory of Loess and Quaternary Geology, Institute of Earth Environment, Chinese Academy of Sciences, Xi'an 710061, China
[c] State Key Laboratory of Environmental Geochemistry, Institute of Geochemistry, Chinese Academy of Sciences, 99 Lincheng Road West, Guiyang, Guizhou 550081, China
[d] Center for Excellence in Quaternary Science and Global Change, Chinese Academy of Sciences, Xi'an 710061, China
[e] Shaanxi Key Laboratory of Accelerator Mass Spectrometry Technology and Application, Xi'an AMS Center, Xi'an 71061, China

ARTICLE INFO

Keywords:
North American westerly jet stream
Laurentide ice sheet
North America-Asian teleconnection
Asian monsoon evolution: Intra D-O/Heinrich scale climate change

ABSTRACT

Compilation of North American loess, dune, lacustrine, and glacial moraine morphological records at places along the retreating Laurentide Ice Sheet shows intra D-O/Heinrich-scale climate oscillations between 28,000 and 10,000 calibrated years before present (calBP). Grayscale variations of the loess-paleosol record that represents the composite stratigraphy reflect the poleward-equatorward displacement of westerly jet stream, associated with advance-retreat of the Laurentide Ice Sheet, both of which superpose on a 2-stage trend of drastic changes. Compilation of paleo-Asian monsoon records from NE, East Central, and SW China also shows a 2-stage evolution of Asian monsoon rainbelt distribution with patterns on intra D-O/Heinrich scales between 28,000 and 10,000 calBP. In stage 1, Asian monsoon rainfall intensity decreases over NE/SW but increases over EC, then drastically fluctuates over NE/SW and keeps constant over EC China. In stage 2, Asian monsoon rainbelts distribute a modern-synoptic-style tripole and reversed tripole mode during boreal interstadials and stadials. Additional compilation of more paleo-Asian monsoon rainfall records and state-of-the-science model precipitation records confirms these patterns over large geographic region and Asian continent during this period. The comparison of global climate forcing factors excludes Atlantic Meridional Overturning Circulation but suggests poleward-equatorward displacements of North American westerly jet streams coupled with ice sheet margin fluctuations at middle to upper midlatitudes, which altered the structures of Eurasian jet streams, to modulate the 2-stage intra D-O/Heinrich-scale changes on Asian monsoon evolution. The drastic retreating of the Laurentide Ice sheet during the second stage made the modern-synoptic-style monsoon rainbelt distribution with seesaw patterns on intra D-O/Heinrich warm and cold phases prominent at 16,000 calBP.

1. Introduction

In Northern Hemisphere, the tropospheric Westerly Jet Stream (WJS) steers global rainbelts migration (Reiter, 1963; Ramage, 1971; Liang and Wang, 1998; Xue and Zhang, 2017). Changes of the Asian WJS control the intensity and locations of Asian monsoon rainfall events (Yeh et al., 1959; Lau and Li, 1984; Lin and Lu, 2005; Li et al., 2005a; Sampe and Xie, 2010; Chiang et al., 2020). Poleward-equatorward displacements of the modern and paleo-North American WJS alternated dry to wet and wet to dry conditions over parts of North America (Trenberth and Guillemot, 1996; Wang et al., 2012; Oster et al., 2015; Putnam, 2015), while spatially asymmetric patterns of Eurasian rainbelts are guided by the wave structure of the tropospheric WJS (Yeh et al., 1959; Liang and Wang, 1998; Chiang et al., 2017; Xue and Zhang, 2017). One teleconnection of North American-Asian atmospheric circulations is that the split of tropospheric polar front and subtropical WJSs over North America often corresponds to a merge of the WJS over East Asia and vice versa (Strong and Davis, 2008).

Merges of Asian subtropical and polar front WJSs intensify jet streams with waves and eddies over the northwestern Pacific region

* Correspondence to: H. Wang, Interdisciplinary Research Center of Earth Science Frontier, Beijing Normal University, Beijing 100875, China.
** Correspondence to: Z. An, State Key Laboratory of Loess and Quaternary Geology, Institute of Earth Environment, Chinese Academy of Sciences, Xi'an 710061, China.
E-mail addresses: hongwang@bnu.edu.cn (H. Wang), anzs@loess.llqg.ac.cn (Z. An).

https://doi.org/10.1016/j.earscirev.2021.103558
Received 4 August 2020; Received in revised form 2 February 2021; Accepted 9 February 2021
Available online 13 February 2021

(Cressman, 1981; Ren et al., 2010, 2011), which consequently modulate low and high atmospheric pressure systems over the midlatitudes of the Asian continent (Nakamura and Huang, 2018). On the feedback, low- and high-pressure systems further steer the direction of WJS propagation causing its troughs and ridges meandering in particular regions to form monsoon rainfall anomalies (Berggren et al., 1949; Rex, 1950a, 1950b; Li and Wang, 2003; Woollings et al., 2010; Boers et al., 2019). During the glacial period, because drastic changes of the Laurentide Ice Sheet had the first-order mechanic forcing on midlatitude westerly flow (Bromwich et al., 2004, 2005), substantial changes of paleo-North American WJSs could influence the downstream Eurasian WJSs and thus Asian monsoon rainfall intensity and spatial patterns.

To better understand how North American WJSs with the ice sheet marginal fluctuation impacted the Asian monsoon rainfall behavior, we compiled climate stratigraphies of loess-paleosol, dune-wetland, marl-lacustrine, and advance-retreat of the Laurentide Ice Sheet at southern margins following its retreating trajectory between 28,000 and 10,000 calBP to synthesize a WJS proxy. The underline hypothesis is that the poleward migration of the subtropical WJSs brought warm rainfall from the Pacific and Atlantic Oceans and the Gulf of Mexico toward the ice sheet, melting back its southern margins and favoring soils and fresh watersheds formation (Bromwich et al., 2004, 2005; Wang et al., 2003, 2012, 2013; Lowell et al., 1999; Heath et al., 2018). On the other hand, the equatorward migration and/or bulging of the polar WJSs caused the ice sheet advance (Wunsch, 2006), creating formidable obstacles for the northward migration of the moisture-laden subtropical WJS (Bromwich et al., 2004, 2005) and favoring loess, dunefield, and salty watershed formation (Wang et al., 2003, 2012, 2013). Their composite climate

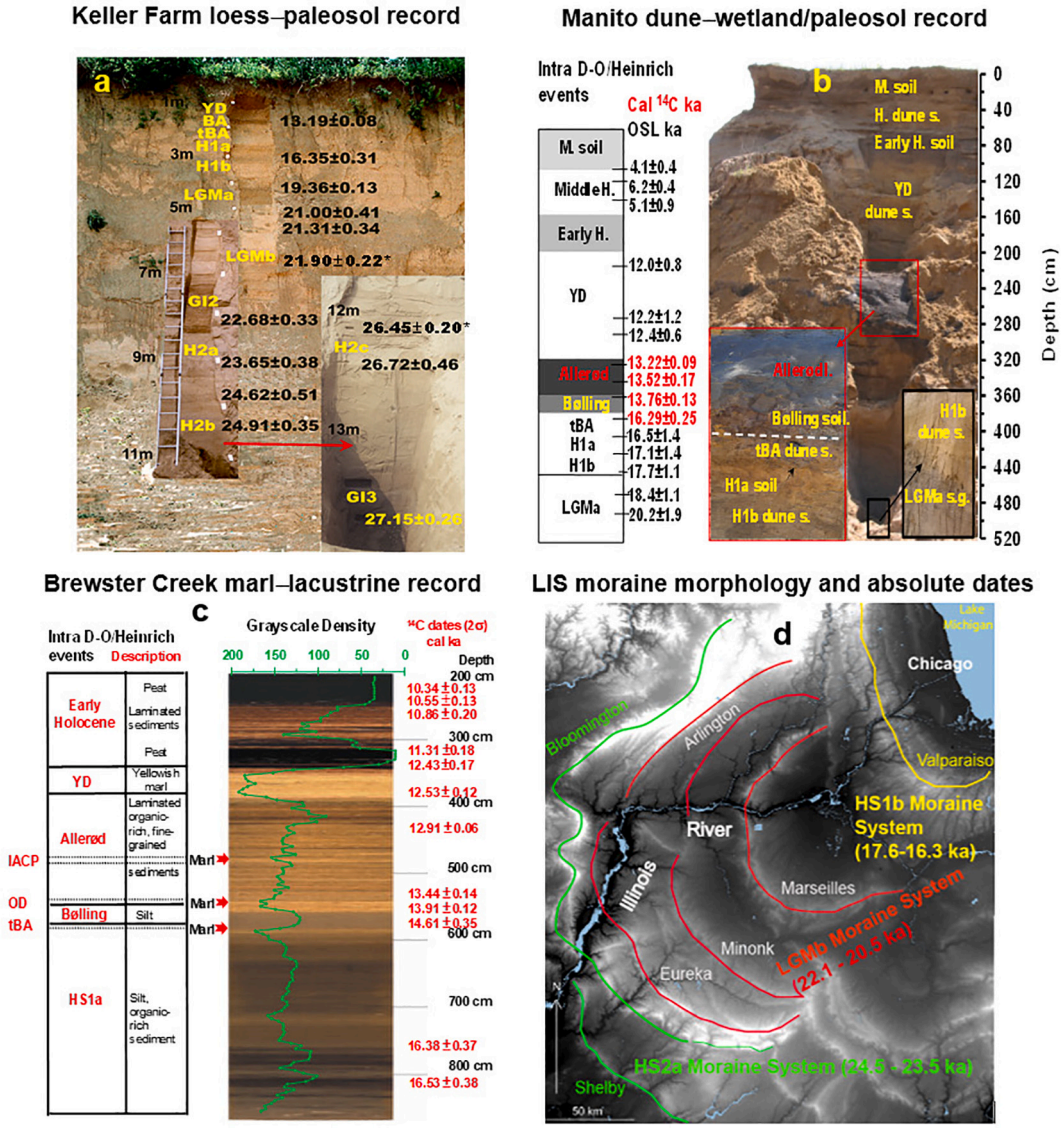

Fig. 1. a. The Keller Farm loess–paleosol succession with ^{14}C dates of low molecular weight soil organic carbon compounds showing intra D-O/Heinrich events since the Greenland Interstadial 3 (GI3) (Wang et al., 2000, 2003); b. The Manito dune–wetland succession with ^{14}C and OSL dates showing intra D-O/Heinrich events since the late Last Glacial Maximum (LGMa) (Wang et al., 2012), black box showing contact between the LGMa and the early Heinrich Stadial 1 (HS1b) units, red box showing HS1b, HS1a, tB/A (transition to Bølling/Allerød), Bølling, and Allerød units, s: sand; g: gravel; c. The Brewster Creek marl–lacustrine succession on AMS ^{14}C chronology showing intra D-O/Heinrich events since HS1a (Curry et al., 2007; Wang et al., 2013), and grayscale variation obtained on the image of this record perfectly characterizes stratigraphic changes; d. The LIS moraine morphology succession with AMS ^{14}C dates of plant leaves, outer 2 rings of a tree stump, and alpha cellulose of the same stump indicating that the Shelby-Bloomington ice (green) advanced to the outermost margins during the HS2a, the Eureka-Arlington-Minonk-Marseilles ice (red) and Valparaiso (yellow) ice advanced to 2nd (3 margins meaning at least 2 short-lived ice margin retreats, see Section 2.4.2. section for further discussion) and 3rd outermost margins during the LGMb and HS1b intra D-O/Heinrich phases (Curry and Petras, 2011; Curry et al., 2018; Table 1). (For interpretation of the references to colour in this figure legend, the reader is referred to the web version of this article.)

stratigraphies are thus synthesized here to reflect the poleward-equatorward displacement of the North American WJS and associated retreat-advance of the Laurentide Ice Sheet at its southernmost margins. It is worth to note that the Midwestern USA is the best area to establish the WJS proxy over the Northern Hemisphere due to no monsoon nor Mediterranean-like seasonal precipitation patterns, which could be steered by different mechanisms. We further compiled paleo-Asian monsoon records over NE, EC, and SW China with reliable chronology and additional records with reliable chronology but shorter sequences with state-of-the-science model precipitation records between 20,00 and 11,000 calBP over N and S China and S Asia (He et al., 2021) to highlight the pattern of the Asian monsoon rainfall behavior between 28,000 and 10,000 calBP. It is noted that changes of high- and low-pressure systems from place to place over the Europe and West Asia in response to changes of North American WJS should have also placed additional forcing factors steering Asian monsoon rainbelts and impacting Tibetan mountain glaciers, and thus detailed Europe/West Asia WJS records should be examined in the future. Here, our comparison of the North American WJS, the Laurentide Ice Sheet margin fluctuation, the Atlantic and Pacific Meridional Overturning Circulation, the Greenland temperature, the boreal summer insolation, and the atmospheric CO_2 concentration records provides new clues for the forcing mechanism for the Asian monsoon rainfall evolution.

2. Geological settings, methods, and results of north American records

2.1. Background of North American records

The loess-paleosol (38°45′ N; 90°00′ W; Wang et al., 2003), dune-wetland (39° 52° N, 90° 22° W; Wang et al., 2012), marl-lacustrine (41°58′ N; 88°16′W; Curry et al., 2007; Wang et al., 2013), and moraine morphology of the Laurentide Ice Sheet at 39–42° N (Frye and Willman, 1960, 1973; Hansel and Johnson, 1986, 1992, 1996; Hansel and Mickelson, 1988; Curry et al., 2018; Dalton et al., 2020) show abrupt warmer/wetter and colder/drier climate oscillations from place to place within the central USA (Figs. 1, 2). While paleosol and organic-rich swamp and lacustrine sediments near ice margins were formed under poleward displacement of the subtropical WJS that brought warm precipitation from the Pacific/Atlantic Oceans and the Gulf of Mexico, loess, dune sand, and alkaline marl deposits were formed under the equatorward displacement of the subtropical and polar front WJS that brought cold/dry airmass (Wang et al., 2000, 2012; Fig. 2). Their composite climate stratigraphy compiled from places on the retreating trail of the Laurentide Ice Sheet functions as a unique proxy indicating the poleward-equatorward displacement of the North American WJS that is associated with the advance-retreat of the Laurentide Ice Sheet margins over midlatitudes. Because the grayscale index on the images of the loess-paleosol outcrops (Wang et al., 2000) characterizes their alternating units in nearly a perfect sense, we borrowed the grayscale index as the WJS proxy.

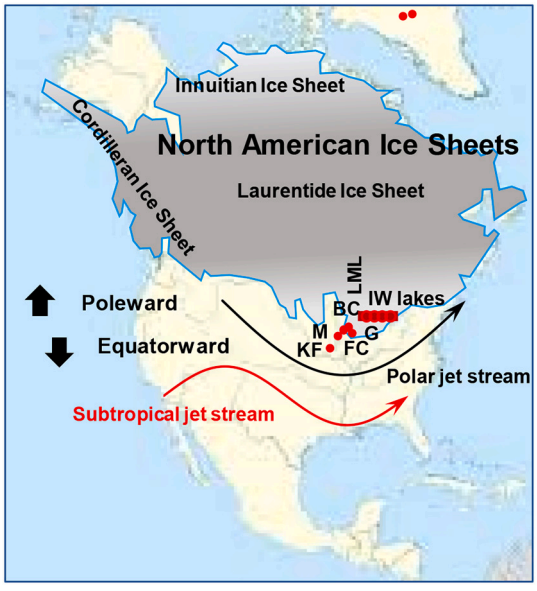

Fig. 2. Locations of compiled sites and Greenland ice records in relative positions to the Lake Michigan Lobe (LML) of the Laurentide Ice Sheet southernmost margins with 3 North American Ice Sheets margins indicated. The schematic diagram showing the poleward-equatorward displacement of the westerly jet streams. KF: The Keller Farm loess site; M: The Manito dune site; FC: The Farm Creek loess site; BC: The Brewster Creek lacustrine site; G: The Gardena silt site; IW: The ice-walled lakes on the Wisconsin Episode Ice-Walled Lake Plain.

Such a view of the poleward-equatorward displacement of the North American WJS and associated rainbelt shifts during the last glaciation is corroborated by the synthesized compilation of large numbers of North America records (Wang et al., 2012). For examples, in parts of the northern USA, the Brady Soil from Nebraska (Mason et al., 2008; Muhs et al., 2008), the $\delta^{13}C$ record from Missouri (Dorale et al., 2010), the dune records from Illinois (Miao et al., 2010; Wang et al., 2012) and Ohio (Campbell et al., 2011), the pollen records from New Jersey and Connecticut (Peteet et al., 1993), and the long-chain fatty acid δD record from Massachusetts (Hou et al., 2006) all indicate boreal cold/dry HS1/YD but warm/wet B/A intervals. In parts of the southern USA the spring-fed black mats record from southwest California-Nevada (Quade et al., 1998), the stalagmite $\delta^{18}O$ record from Arizona (Wagner et al., 2010), the stalagmite $\delta^{18}O$ record from New Mexico (Asmerom et al., 2010), the different stalagmite growth rate records from the central Texas (Musgrove et al., 2001), the stalagmite $\delta^{18}O$ record from the Alabama (Lambert et al., 2010), and the pollen record from Florida (Grimm et al., 2006) all indicate cool/wet HS1/YD but warm/dry B/A intervals. These records suggested that the North American WJSs controlled the rainbelts distribution on a seesaw patterns between the North and South USA during last glacial-period abrupt climate changes (Wang et al., 2012).

2.2. Methods for the North American WJS proxy

The lightness L* variation (=grayscale density) was measured on the images of the Keller Farm loess-paleosol outcrops using the method described in Wang et al. (2013) to characterize the physical change of the alternating loess and paleosol unit. Specifically, we drew three 5 × 5-pixel boxes horizontally on the Photoshop (Software) image of the Keller Farm loess-paleosol outcrops to measure the relative changes of the L* values at multiple spots, and measurement was carried out from the top to the bottom of the outcrop in a 5-pixel increment. An average value of L* value with 1σ uncertainty was taken from multiple measurements, which is plotted to represent the composite climate stratigraphy (Fig. 3).

2.3. Definition of the intra D-O/Heinrich scale climate stratigraphy

The compilation of the composite climate stratigraphy over the central USA shows that so called “super-cold” HS2, LGM, and HS1 stratigraphies near the Laurentide Ice Sheet margins are commonly punctuated by one or more sub-chronozones with clear warming features, e.g. the HS2, LGM, and HS1 stratigraphies show 3, 2, and 3 alternating cold and warm sub-facies (Figs. 1, 3).

These observations are generally consistent with the observations that “super-cold” North Atlantic Heinrich Stadials (Broecker et al., 1992) contain warm climate signals, as indicated by the Laurentide Ice Sheet retreats at multiple lobes (Lowell et al., 1999; Heath et al., 2018). To avoid confusing when implementing more detailed comparison study between the Atlantic basin Heinrich event with other time-equivalent climate events, here we used the intra D-O/Heinrich-scale climate stratigraphic concept to describe these Greenland stadials.

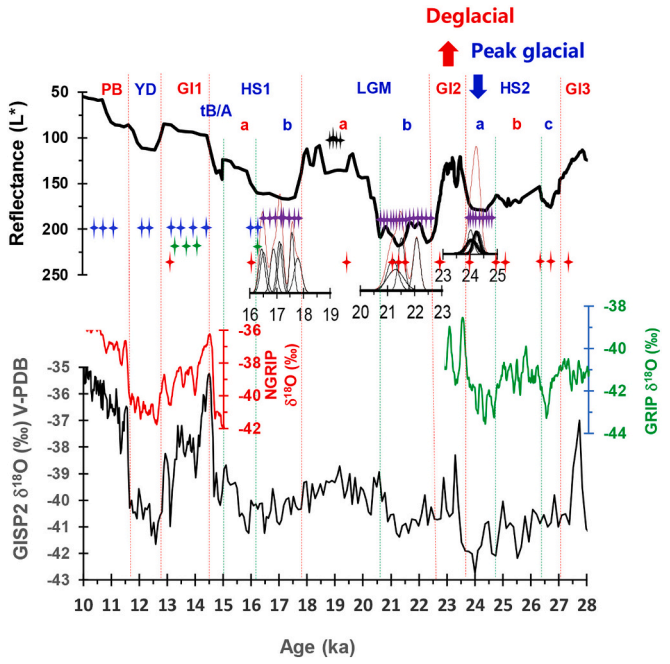

Fig. 3. Definition of intra D-O/Heinrich-scale climate changes in records of the loess-paleosol L* index that represents the composite climate stratigraphy of the loess, dune, lacustrine, and glacial moraine records in the central USA and of the GISP2, GRIP and NGRIP $\delta^{18}O$ records that indicate the Greenland air temperature changes between 28,000 and 10,000 calBP. Intra phases are observed particularly in the boreal cold interval: the HS2 is divided into a, b, c 3 intra phases with the LIS advancing to its southernmost margins during the HS2a interval, defined as the peak glacial; the LGM is divided into a and b 2 intra phases with the LIS advancing to its second southernmost (several) margins during the LGMb interval; the HS1 is divided into tBA, a, b 3 intra phases with the LIS advancing to its third southernmost margin during the HS1b interval over the central USA. The GI2 interstadial is named as the default deglacial for the discussion. A total of 64 radiocarbon dates was compiled from 893 radiometric database (Curry et al., 2018). They include i) 4 (black), ii) 32 (purple), and iii) 11 (blue) accurate plant fossil AMS radiocarbon dates with cumulative probability, iv) 4 (green), and v) 13 (red) high temperature pyrolysis radiocarbon dates for the chronology of i) the LGMa-aged meltwater flood (see Kankakee Torrent story in Curry et al., 2014); ii) the HS2a-, LGMb-, and HS1b-aged LIS advances, and 3) the marl-lacustrine climate stratigraphic record; iv) the dune-paleosol, and v) the loess-paleosol records (Wang et al., 2003, 2012). The cumulative curves of probability of accurate fossil plant AMS radiocarbon dates provide reliable age controls for the timing of cold HS2a, LGMb, and HS1b intra-phases and thus the warm phases in between, which provide ideal tie points for transferring the GISP2 and GRIP chronologies to the North American WJS record. (For interpretation of the references to colour in this figure legend, the reader is referred to the web version of this article.)

2.4. Chronology of the intra D-O/Heinrich-scale climate stratigraphy

2.4.1. Chronology of the advance-retreat of the LML of the Laurentide Ice Sheet

AMS ^{14}C dates were selected to synthesize the reliable chronology of ice margin deposits from: 1) terrestrial fossil plants in proglacial lakes and paleosol horizons immediately underpin the ice margin deposit for maximum ages of the ice advance; 2) cold-climate adapted terrestrial.

fossil plants from ice-walled lake deposits on the late Wisconsin Episode till plain for the onset of the ice advance. It is noted that cold-adapted terrestrial fossil plants preserved in the ice-walled lacustrine may represent the ice front stagnant with kind of warming signals because the super-cold condition for the intense ice sheet advance should not support any kind of plants to grow on the surface of the ice sheet. But at its southernmost margins the ice sheet was relatively thin and sensitive to short-lived warming events within the ice advance interval, and we argue that cold-adapted terrestrial fossil plants prevailed in ice-walled lakes on ice margin deposits can be used to indicate ice sheet advance in a broad sense. From recently recompiled 893 ^{14}C dates (Curry et al., 2018; www.geosociety.org/ datarepository/2018/), terrestrial fossil plants, insect nest, outer 2 ring α-cellulose of a tree stump that was cut by the advancing ice sheet were selected for the abovementioned category 1) database. These chronologies reveal that the outermost Bloomington and Shelby Moraine systems of the LML of the Laurentide Ice Sheet occurred during the HS2a intra phase (Fig. 1d; Table 1). Cold-climate adapted fossil plant leaves and needles were selected for the category 2) database. These chronologies reveal that the 2nd (several) outermost Eureka-Arlington-Minonk-Marseilles Moraine systems occurred during the LGMb, and the 3rd outermost Deer Plainfield-Tinley-Valparaiso Moraine systems occurred during HS1b intra phases (Fig. 1d; Table 1). The cumulative probability curves of AMS ^{14}C dates newly calibrated on IntCal20 here confine timings of ice sheet advances during HS2a, LGMb, and HS1b intra-phases and retreats in between (Fig. 4).

2.4.2. Chronology of the loess–paleosol record

The loess–paleosol succession at the Keller Farm site in the middle Mississippi River valley was located 120 km southwest of the outermost ice margin during the HS2a intra phase, a place not too far or too close to the ice margin with relatively higher resolution of both pedogenesis and loess accumulation profiles in the stratigraphy (Fig. 1a). The striking difference between brighter, carbonate-rich, coarse-grained loess layers and darker, iron oxide-stained, finer-grained paleosol horizons reveals alternating cold/dry and warm/wet climatic regimes (Wang et al., 2000, 2003). With the reasonably-constrained conventional ^{14}C chronology through high-temperature pyrolysis pretreatment method (Wang et al., 2000, 2003), loess layers were found in HS2c, HS2a, LGMb, HS1b, tBA, and YD cold intervals, whereas paleosol horizons were found in GI3, GI2, HS2b, LGMa, HS1a, and GI1 (Bølling/Allerød) warm intervals (Fig. 1a).

At the Keller Farm loess site, the GI2 paleosol complex is well developed with the profound bioturbation feature in the top and bottom horizons recognizable, which conceptually matches double peaks of Greenland ice $\delta^{18}O$ record (Figs. 3, 5a). Weak but recognizable paleosol horizons in the super-cold LGMb interval (Figs. 1a, 5a) with supportive evidence of 3 LGMb-phased moraine systems of the Eureka-Arlington-Minonk-Marseilles (Fig. 1d), suggest at least 2 short-lived ice-margin retreats or short-lived warmer/wetter conditions during the general cold LMGb intra phase (Fig. 5a). These intra D-O/Heinrich climate stratigraphic units are fully in-phase with the LML of the Laurentide Ice Sheet advance and retreat within the dating uncertainties.

Because the HS2b-phased paleosol horizon is poorly recognizable at the Keller Farm loess site due to leaching-induced depletion of clays and iron minerals by groundwater saturation, a well-positioned paleosol horizon that is overlain by the HS2a-aged ice margin deposit of the Tiskilwa Till along the Bloomington Moraine (Fig. 1d) near the Gardena site (Fig. 2) is presented here to corroborate the abrupt change from the warm/humid paleosol horizon to cold/dry glacial deposit (Fig. 5b). In other words, the succession of the Tiskilwa Till stratigraphy (HS2a-phased glacial deposits) over the well-observed paleosol horizon with a moss layer on the top, developed in the Morton Loess, provides direct evidence for the abrupt climate transition from a relative warm regime to the rigid cold regime (Fig. 5b). It is noted that at 1 km northwest of the Gardena site, the Morton Loess at the Farm Creek exposure shows a dolomite-rich and coarse-silt zone (= HS2c) immediately below the marker bed of the moss layer-paleosol horizon (HS2b) (Fig. 5c). These loess and glacial stratigraphic records in the central USA consistently reveal that the HS2 interval experienced cold-warm-cold intra D-O/Heinrich scale climate changes.

2.4.3. Chronology of the dune–wetland/paleosol record

In the middle Illinois River valley, the Manito dune–wetland/

Table 1
Selected AMS and radiometric ^{14}C dates of fossil plants and wood fragments from 893 ^{14}C age database (Curry et al., 2018; www.geosociety.org/ datarepository/2018/) for ice margin advances of the Lake Michigan Lobe of the Laurentide Ice Sheet.

Lab #	Material	^{14}C age	± 1σ	calBP IntCal20*	±2σ
HS1b phase					
Tinley Moraine (Valparaiso Moraine system), ice-walled lake plain; tundra plants					
UCIAMS-26262	stems, leaves	14,070	40	17,125	155
UCIAMS-26263	stems, leaves	14,110	35	17,185	145
UCIAMS-26264	stems, leaves	14,420	40	17,585	215
Deerfield Moraine (Valparaiso Moraine system), ice-walled lake plain; tundra plants					
UCIAMS-46829	stems, leaves	13,650	40	16,485	160
UCIAMS-63075	stems, leaves	13,695	45	16,560	200
UCIAMS-63076	stems, leaves	13,910	35	16,930	155
LGMb phase					
Marseilles Moraine (Marseilles Moraine system), ice-walled lake plain; tundra plants					
UCIAMS-157641					
ISGS A3495	stems, leaves	16,800	70	20,320	185
UCIAMS-157642					
ISGS A3496	stems, leaves	16,760	70	20,270	200
UCIAMS-157643					
ISGS A3497	leaves	16,910	70	20,435	175
UCIAMS-157644					
ISGS A3498	stems	17,040	80	20,595	205
UCIAMS-157645					
ISGS A3499	stems	17,130	80	20,685	185
UCIAMS-157647					
ISGS A3501	stems	17,440	70	21,035	230
UCIAMS-26260	stems, leaves	17,760	60	21,585	245
UCIAMS-26261	stems, leaves	18,210	60	22,170	150
Arlington/PawPaw Moraine (Marseilles Moraine system), ice-walled lake plain; tundra plant					
UCIAMS-97040	stems, leaves	17,560	50	21,200	200
UCIAMS-97068	stems, leaves	18,080	90	22,030	250
Champaign Moraine, proglacial lake, tundra plants					
UCIAMS-46838	stems, leaves	17,695	45	21,430	280
UCIAMS-46839	stems, leaves	17,730	470	21,475	1120
HS2a phase maximum age: by dates of organic remains from HS2b phase					
Shelbyville Moraine; proglacial lake, wood fragments from Charleston Quarry					
ISGS-2842	wood stump	19,980	150	24,015	310
ISGS-2593	wood	20,050	170	24,080	380
UCIAMS-155338					
ISGS-A3363	outer 2 rings				
of wood stump	20,480	70	24,640	310	
UCIAMS-157639					
ISGS-A3493	α-cellulose of wood stump	20,590	110	24,805	380
Bloomington Moraine; proglacial lake, fossil plants, insect nest, moss from Farm Creek					
UCIAMS-142908					
ISGS A3136	plant needles	19,960	70	23,970	185
UCIAMS-142911					
ISGS A3139	bud/bract/ moss	20,170	80	24,195	290
UCIAMS-142910					
ISGS A3138	bud/bract/ moss	20,230	70	24,290	255
UCIAMS-142911					
ISGS A3139	nest caddisfly	20,160	80	24,180	290
HS2a phase: Madison/Pike/Madison Co.: Sunset Hill/Kiser Creek/Keller Farm					
ISGS-129	peat	19,750	500	23,780	1190
ISGS-3300	Wood trigs	19,650	620	23,680	1400
ISGS-3939	Py-V SOC	19,640	310	23,590	680

*Reimer et al., 2013.
**ISGS Radiocarbon Dating lab collaborates with University of California AMS Radiocarbon Dating lab for the early study. Note: ISGS lab code with "A" for AMS ^{14}C dates (new information in this study) is also provided here, which was not provided in Curry et al. (2018; www.geosociety.org/ datarepository/2018/), along with the UCIAMS AMS code. ISGS code without "A" is a radiometric ^{14}C date.

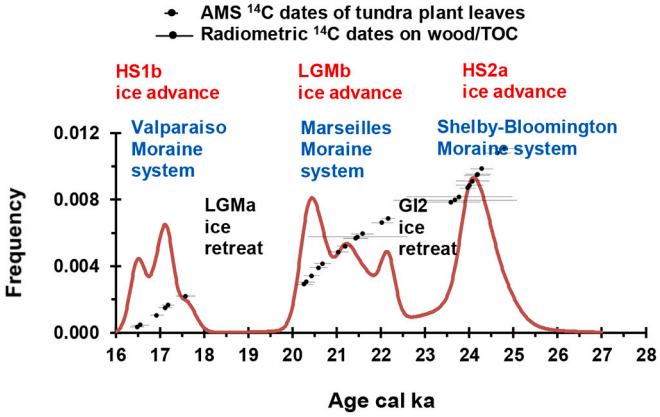

Fig. 4. Cumulative curves of the probability density function of AMS and radiometric ^{14}C dates (Table 1) indicating ice margin advance and decay. For HS2a-phased ice advance and duration, averaged-maximum AMS ^{14}C dates with other ^{14}C dates of HS2a-equivalent sediment are compiled. Note: one AMS ^{14}C date has a large uncertainty (Table 1).

paleosol succession was located 50 km southwest of the 2nd outermost or LGMb-aged ice margins. With high temperature pyrolysis ^{14}C dates of wetland and paleosol horizons and optically stimulated luminescence dates on eolian sand, the dunefield in this area was active during the HS1b, tBA, and YD cooling intervals, and the meltwater flood-introduced basial outwash, warmer/wetter climate introduced wetland and paleosol stratigraphic units occurred during the LGMa, HS1a, Bølling/Allerød, and early Holocene warm intervals (Wang et al., 2012; Fig. 1b). The absence of LGMb-aged and older glacial sediments at this site most likely resulted from erosion by the large meltwater discharge during the LGMa warm phase. These intra D-O/Heinrich climate stratigraphic units since the LGMa are fully in-phase with the Keller Farm loess–paleosol and Laurentide Ice Sheet advance and retreat records within the dating uncertainties (Wang et al., 2012). Intriguingly, the obvious erosion surface between the Bølling equivalent wetland soil and Allerød equivalent lacustrine units here indicates a sedimentological hiatus, by default it could reflect the Older Dryas (OD) cold snap in the Midwest dunefield (Fig. 6).

2.4.4. *Chronology of the marl–lacustrine record*

On the Wisconsin Episode till plain in northeast Illinois near Chicago area, the Brewster Creek marl–lacustrine succession was situated on the 3rd outermost ice margin (Curry et al., 2007). The basal unit at this site is the organic-rich HS1a equivalent lacustrine deposit, when the retreating Valparaiso (3rd) ice margin was located about 50–100 km northeast in the Lake Michigan basin. The HS1b and older deposits were not preserved, assumingly truncated by the Valparaiso ice advance to this site during the HS1b phase and/or eroded away by the later phase meltwater floods. Twelve AMS ^{14}C dates of terrestrial fossil plant leaves and needles were obtained at this site for the reliable chronology synthesis (Curry et al., 2007; Wang et al., 2013). The HS1a-phased lacustrine, thin tBA marl (short-duration marshland), Bølling lacustrine, thin OD marl, laminated Allerød lacustrine (littoral lake), thin but observable Inter-Allerød-Cold-Period (IACP) marl, thick YD marl (prolonged marshland), and early Holocene peat (swamp) deposits were interpreted to indicate warmer/wetter and colder/drier climate changes on the intra D-O/Heinrich scales (Fig. 1c; Wang et al., 2013). This is an astonishing record in which both OD and IACP intervals were not only recognizable

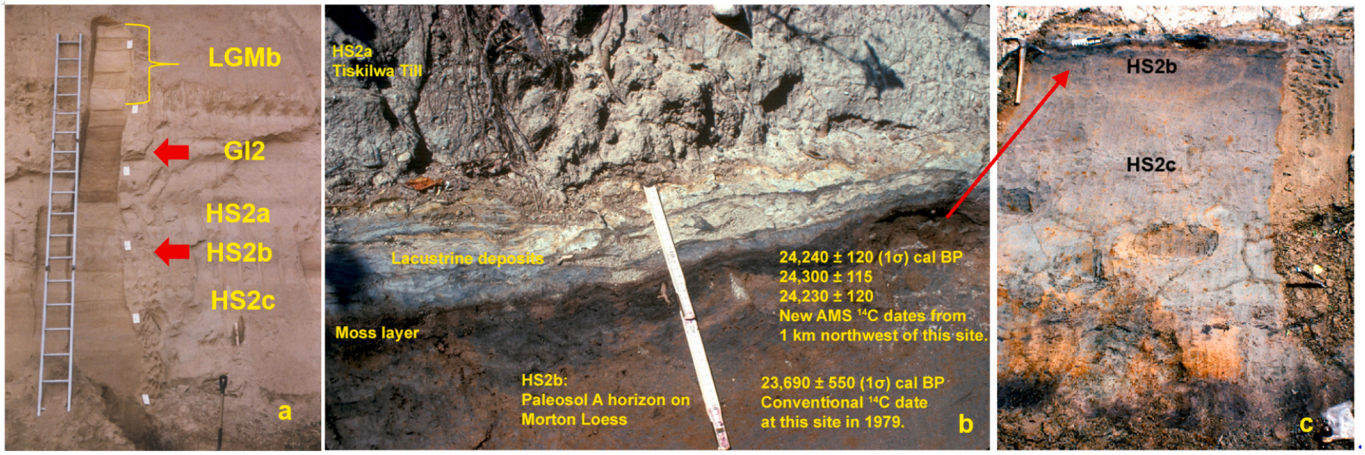

Fig. 5. a. The middle Keller Farm loess exposure showing the GI2 equivalent paleosol complex with prominent soil horizons on the top and bottom matching double peaks of the GI2 interstadial event in the GISP2, GRIP, and NGRIP $\delta^{18}O$ records. The overlying LGMb loess unit containing 2 incipient paleosol A horizons and the underlain loess unit showing soil carbonate-faded horizonation of HS2a, HS2b, and HS2c intra phases; red arrows indicating warm intervals; b. The Gardena Section showing the HS2a equivalent glacial Tiskilwa Till overlying HS2b equivalent paleosol horizon with a moss layer on the top, which was developed into the Morton Loess. One conventional ^{14}C date in 1979 on a mixture of wood and moss remains yielded a calibrated ^{14}C age of 23,690 ± 550 BP (Follmer et al., 1979). Recent fossil plant, moss, and nest of caddisfly samples from the same stratigraphic unit in the Farm Creek Section, 1 km northwest of the Gardena Section providing accurate and precise AMS ^{14}C dates for the maximum age of the HS2a-aged Tiskilwa Till and HS2b-aged paleosol unit, consistent with the early radiometric ^{14}C date within 2σ uncertainty. c. Farm Creek section showing the Morton Loess with the HS2b-phased moss layer-paleosol profile, and dolomite-rich and coarser silt deposits at the lower profile showing the cold/dry HS2c-phased loess unit gradually changed to warm/humid HS2b-phased paleosol horizon. Photo courtesy of b, c to Dr. Leon Follmer. (For interpretation of the references to colour in this figure legend, the reader is referred to the web version of this article.)

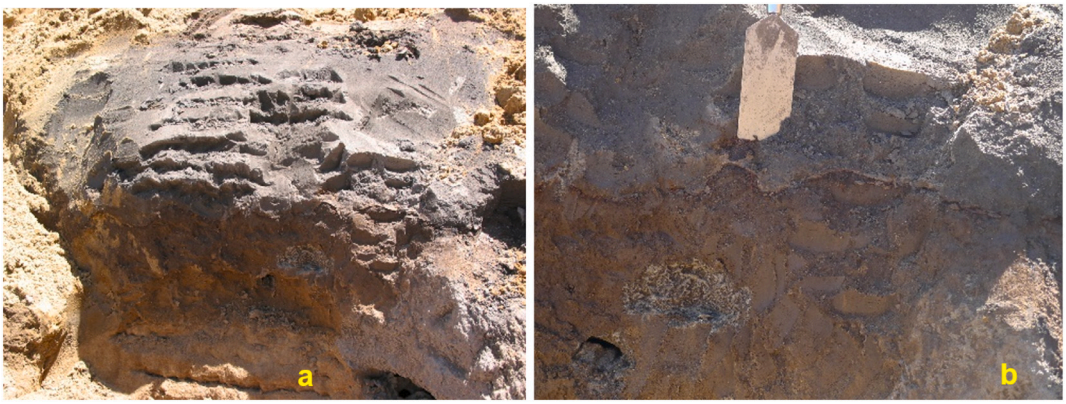

Fig. 6. a. Middle Manito dune-wetland/paleosol exposure showing reddish Bølling-aged prominent paleosol and dark organic-rich Allerød-aged wetland unit. b. an iron crest between Bølling and Allerød equivalent units showing a sediment hiatus and intensive weathering zone, which is interpreted as the default Old Dryas equivalent climate stratigraphic unit (Wang et al., 2012).

but also measurable in addition to the HS1 and GI1 records, and the reliable AMS ^{14}C dates of fossil plants from this site (Curry et al., 2007) indeed corroborate the presence of the intra D-O/Heinrich events in nearby loess and dune successions and the advance and retreat of the LML of the Laurentide Ice Sheet on the same time scales.

2.4.5. *Method of establishing reliable regional chronology*

It is notoriously difficult to establish a reliable ^{14}C and OSL chronology for loess-paleosol and dune-paleosol sequences, while terrestrial fossil plants most likely preserved in lake deposits can provide accurate AMS ^{14}C chronology. However, stratigraphic changes between loess/dune layers and paleosol horizons visually clarify context of climate changes and any chemical and physical parameters, as long as they characterize the stratigraphy, can be borrowed as reliable climate proxies. On the other hand, lacustrine time series depends heavily on the establishment of the climate proxy, a challenging process due to complicated hydroclimate conditions, requiring independent test for the integrity. Since uncertainties of ^{14}C and OSL dates on total organic carbon and sand grains are too large to identify closely-spaced climate stratigraphic units, consecutive intra D-O/Heinrich climate stratigraphies without any missing unit from loess, dune, proglacial lacustrine, and ice-walled lacustrine were selected to establish the regional climate stratigraphic framework. The key of this method is to share the reliable chronology on the lacustrine sequence and clear climate signals on the loess-paleosol sequence between different records. In this case, ^{14}C and OSL dates of loess and dune sequences were only used to identify these climate stratigraphic units, known as the chronozone, which were confirmed by the accurate AMS ^{14}C dates of the sequential chronozones in the lacustrine record. As described above, the complete climate stratigraphic sequence without a single unit missing within a certain time interval provides the confidence for establishing the regional climate stratigraphy.

2.5. *Significance of the intra D-O/Heinrich-scale climate events*

Sixty-four ^{14}C dates were selected including 47 AMS ^{14}C dates of

fossil Dryas, arctic blueberry, arctic willow leaves and conifer needles from recently re-compiled 893 ^{14}C database (Curry et al., 2018) and from additional records for the chronological framework. Composite climate stratigraphy covering different sediment entities in the study region (Fig. 2) shows 13 intra D-O/Heinrich scale chronozones between 28,000 and 10,000 calBP (Fig. 3), which are described as follows: the GI3 is the last warming phase before the peak glaciation, while the HS2 has a, b, c 3 intra phases with the ice sheet advancing to its southernmost margin during the HS2a intra phase, defined as the peak glaciation here (Figs. 1, 2, 3); the GI2 is the first warming phase after the peak glaciation, viewed as the default deglaciation because the Laurentide Ice Sheet has never advanced back to its southernmost margin again after this point; the LGM has a, b 2 intra phases with the ice sheet advancing to its 2nd southernmost (several) margins in the LGMb intra phase (Figs. 1, 2, 3) and with the ice sheet retreating significantly in the LGMa intra phase to Milwaukee, Wisconsin, USA (Dalton et al., 2020); the HS1 has tBA, a, b 3 intra phases with the ice sheet advancing to its 3rd southernmost margin in the HS1b intra phase and then retreating out of study regions permanently, presumably far north of the Milwaukee in the HS1a intra phase; perhaps the Laurentide Ice Sheet advanced again in the tBA intra phase at upper midlatitudes; last 3 intra D-O/Heinrich scale phases are the GI1 interstadial, the YD stadial, and the PB interglacial (Figs. 1, 2, 3).

2.6. North American intra D-O/Heinrich-scale climate changes on the Greenland ice chronology

The compilation shows that these 13 intra D-O/Heinrich phases are exactly identified in the Greenland GISP2 and supplemented by the GRIP/NGRIP δ^{18}O records, suggesting that faster-than D/O/Heinrich climate cycles prevailed widely in the North Atlantic basin and the North American continent (Figs. 1, 3, 4, 5, 6). This allowed us to transfer the GISP2 and GRIP ice chronology to the North American composite climate stratigraphy on the L* index of the Keller Farm loess-paleosol succession, assuming synchronous variation of climate conditions occurred over the Laurentide Ice Sheet southern margins and Greenland. Specifically, ages of each boundary of the 13 intra D-O/Heinrich events from the Greenland GISP2 and GRIP δ^{18}O records were transferred to the loess-paleosol grayscale record with the originally calibrated ^{14}C dates were used only as the reference to identify the intra D-O/Heinrich units. On the other hand, 47 accurate and precise AMS ^{14}C dates of fossil leaves from ice-walled lakes on the last glacial till plain and proglacial lakes near ice margins (Table 1; Figs. 1, 3; Curry et al., 2018) provided the reliable chronology to constrain not only the timing of ice sheet advances as cold events on the loess grayscale index curve but also on the Greenland ice δ^{18}O records as well (Figs. 1, 3, 4). The transformation of the GISP2/GRIP chronology to the loess-paleosol grayscale L* record made the North American composite climate stratigraphy a unique proxy to indicate the poleward-equatorward displacement of the WJS, associated with the retreat-advance of the Laurentide Ice Sheet at its southernmost margins on intra D-O/Heinrich scales between 28,000 and 10,000 calBP.

3. Geological settings, methods, and results of East and Southern Asian records

3.1. Background and methods

Three Asian paleoclimate records all with reliable chronologies spinning between 28,000 and 10,000 calBP across the NE, EC (east central), and SW China and 6 additional classical records with state-of-the-science model precipitation records in N/S China and S Asia between 20,000 and 11,000 (He et al., 2021) were selected for the synthesis (Fig. 7). Although the transient simulation of annual precipitation on 10-year resolution (He et al., 2021) only captures the regional monsoon precipitation patterns on D-O/Heinrich scale during last deglaciation, it can serve testing purpose on Asian monsoon rainfall patterns on intra D-O/Heinrich scales.

In the NE sector of China, changes of total organic content in lacustrine sediment with AMS ^{14}C dates of well-preserved terrestrial fossil plants from Sihailongwan volcanic Lake in Jilin Province at 42°17′ N, 126°36′ E reflect East Asian summer monsoon rainfall intensity over NE China (Mingram et al., 2018). In the EC sector, the variation of the δ^{18}O record with well-dated chronology of Haozhu cave stalagmite in the Hubei Province at 30°41′ N, 109°59′ E reflects East Asian summer

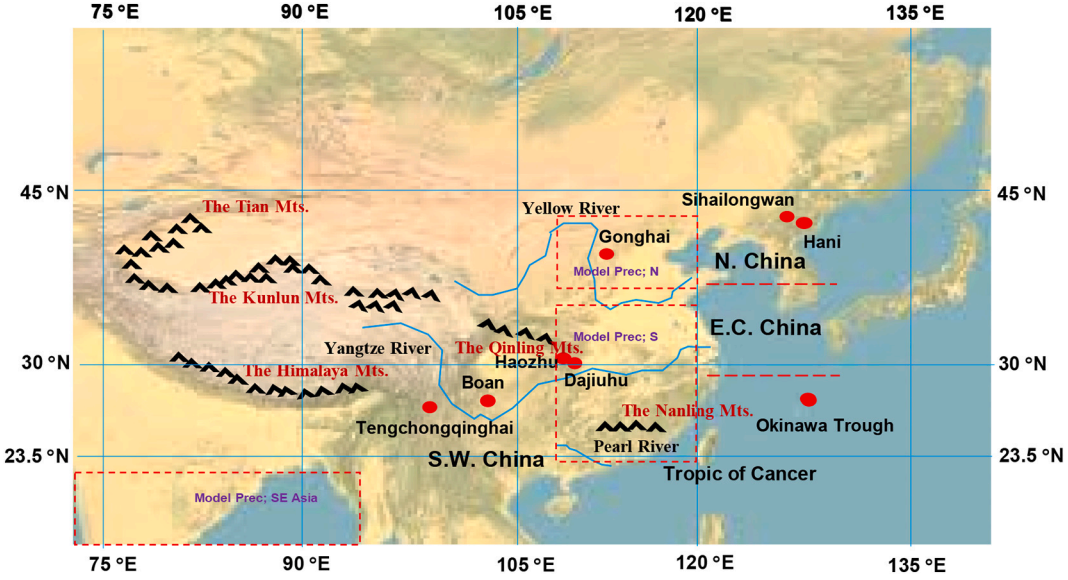

Fig. 7. Locations of 3 paleoclimate records, Sihailongwan volcanic lacustrine, Haozhu cave stalagmite, and Boan lacustrine sites for the synthesis of Asian monsoon rainfall patterns and 6 additional classical records and 3 regions (red dashed rectangle) modeled annual precipitation for last deglaciation (He et al., 2021) as supplementary information for the discussion of the evolution of glacial-period Asian monsoon rainfall behaviors. Haozhu site provides 2 proxies: stalagmite δ^{18}O and Sr/Ca ratio. Model precipitation (prec) in N. Chica in area of 37–43°N/108–120°E, in *S. china* in area of 22–35°N/108–120°E, and in S.E. Asia in area of 10–25°N/70–95°E during last deglaciation (He et al., 2021). (For interpretation of the references to colour in this figure legend, the reader is referred to the web version of this article.)

monsoon rainfall variation over the middle-lower Yangtze River tributary (Zhang et al., 2018). In the SW sector, changes of the cellulose $\delta^{13}C$ values with cellulose AMS ^{14}C dates from the Baoan peat sequence in the Sichuan Province at 28°47′ N, 102°57′ E reflect Indian summer monsoon rainfall variations (Hong et al., 2018). For the additional representation of the geographic regions, 2 records were selected from Northern China: Lake Gonghai pollen-based annual precipitation (Chen et al., 2015) and Hani peat biomarker index (Zhou et al., 2010); 2 records were selected from Central China: Haozhu cave stalagmite Sr/Ca ratio (Zhang et al., 2018) and Dajiuhu peat biomarker records (Xie et al., 2013); 2 records were selected from Southern China: Lake Tengchongqinghai grain size variation (Zhang et al., 2017) and Pollen records from the Okinawa Trough in East China Sea as rainfall intensity index over Southern China (Xu et al., 2013; Fig. 7). We lined up the model precipitation results (He et al., 2021) in areas of 37–43°N and 108–120°E with the NE China sector, in areas of 22–35°N and 108–120°E with the EC sector and in areas of 10–25°N and 70–95°E with the SW China sector because both are Indian monsoon affected regions (Fig. 7).

3.2. Asian summer monsoon rainfall patterns

The compilation reveals that Asian monsoon rainfall intensity over NE, EC, and SW China displays a distinctive 2-stage evolution between 28,000 and 10,000 calBP (Fig. 8). During the stage 1 from 28,000 to 18,000 calBP, Northern Hemisphere experienced extraordinary climate changes from the warm GI3 to coldest HS2a, warm deglacial GI2, supercold LGMb and finally to warm LGMa intra D-O/Heinrich phases (Fig. 8). Asian monsoon rainfall intensity decreases in both NE/SW but increases in EC, and then drastically fluctuated over NE/SW and keeps constant in EC sectors (Fig. 8). During the stage 2 from 18,000 to 10,000 calBP, Northern Hemisphere experienced magnificent-scale climate changes from the cold HS1b to lukewarm HS1a, cold tBA, astonishingly warm GI1, cold YD, and finally hot Preboreal intra phases in a relative sense. Asian monsoon rainbelts clearly distributed reversed tripole rainfall modes during relatively cold boreal HS1 and YD phases, and tripole rainfall modes during warm GI1 and PB phases over NE, EC, and SW sectors of China (Fig. 8). The compilation clearly reveals dry-wet-dry and wet-dry-wet seesaw flips of Asian monsoon rainfall patterns over three sectors of China between cold and warm climate conditions (Fig. 8), which resembles the modern-synoptic-like Asian monsoon rainfall patterns (Ding et al., 2008, 2009). We noted that the extraordinary modern-style asymmetry of Asian monsoon rainfall modes over East Asia begins since 16,000 calBP (Fig. 8). The asymmetry of Asian monsoon rainfall modes over the larger geographical China are further confirmed by compilation of 7 additional classical records including important wetness indicator of Hani peat (Zhou et al., 2010) and Dajiuhu peat (Xie et al., 2013) sequences (Fig. 9). It shows a great consistency of the 2-stage evolution of Asian monsoon rainfall behaviors with profound tripole and reversed tripole patterns of monsoon rainbelt distributions over general North, Central and South China (Figs. 8, 9). It is noted that the variance of the rainfall intensity was low in the stage 1 and extraordinarily high in the stage 2 in all records (Figs. 8, 9).

3.3. Synthesized results controversial with the Asian cave stalagmite $\delta^{18}O$ records

However, it is noted that almost all Chinese stalagmite $\delta^{18}O$ records except for the Haozhu cave proxies (Zhang et al., 2018) show synchronous and uniform rainfall patterns over the vast geographic China throughout up to 8 glacial-interglacial cycles (Wang et al., 2001; Yuan, 2004; Cheng et al., 2016, 2019). The school of stalagmite $\delta^{18}O$ database contradicts the modern synoptic weather systems in terms of asymmetric distributions of summer monsoon rainbelts, which raises concerns of what Asian stalagmite $\delta^{18}O$ values really indicate (Johnson et al., 2006; Clemens et al., 2010; Dayem et al., 2010; Chen et al., 2015; Cheng et al., 2019; Liu et al., 2015; Zhang et al., 2018; Kong et al., 2017;

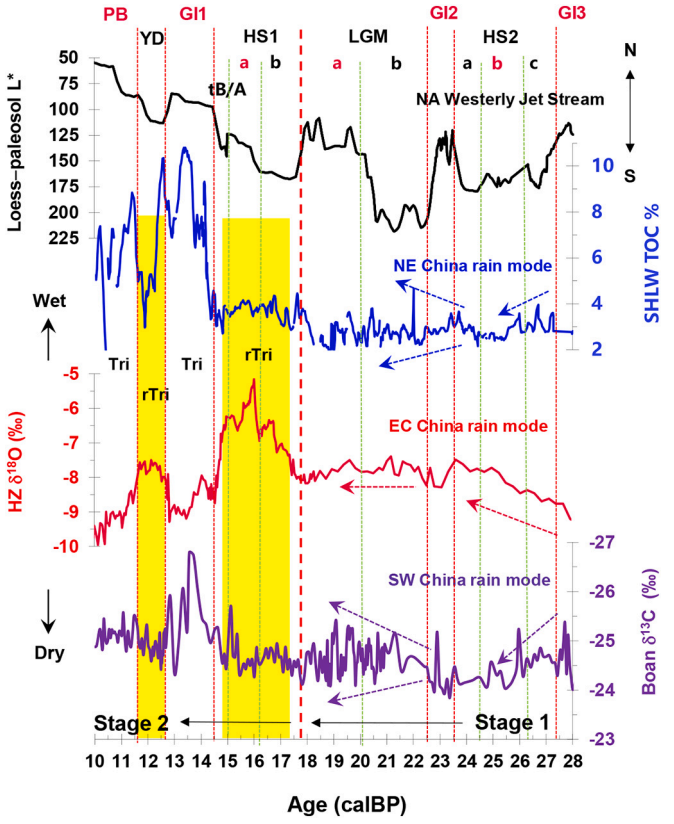

Fig. 8. Proxies of poleward-equatorward displacement of the North American WJS by loess-paleosol L* index (this study) with calibrated to GISP2/GRIP chronologies, NE China rainfall intensity by Sihailongwan lacustrine TOC% values (Mingram et al., 2018), EC China rainfall intensity by Haozhu cave stalagmite $\delta^{18}O$ values (Zhang et al., 2018), and SW China rainfall intensity by Boan peat cellulose $\delta^{13}C$ values (Hong et al., 2018) all with the reliable chronologies. Compilation shows a 2-stage evolution of the Asian monsoon rainfall pattern with subtle changes in-phase with the intra D-O/Heinrich-scale poleward-equatorward displacements of the North American WJS and Laurentide Ice Sheet fluctuations at its southern margins. During the stage 1, Asian monsoon rainfall intensity firstly decreased in both NE/SW but increased in EC China and then fluctuated with a high frequency between strong and weak in NE/SW and remained constant in EC sectors (arrows). During the stage 2, Asian monsoon rainfall distribution displays a profound dry-wet-dry reversed-tripole (rTri) mode during relatively cold HS1 and YD stadials (orange shades) but an extraordinary wet-dry-wet tripole (Tri) mode during relatively warm GI1 and PB interstadial and interglacial over NE, EC, and SW China.

Chiang et al., 2017, 2020; He et al., 2021). Modeling simulation of $\delta^{18}O$ values of seasonal rainfall and stalagmite suggest that asymmetric rainfall patterns occur when normal step-wise north-south migrations of the Asian WJS from late spring to midsummer is collapsed at a certain step due to abnormal climatic boundaries, while Asian stalagmite $\delta^{18}O$ values do not necessarily reflect rainfall intensity (Chiang et al., 2017, 2020; Kong et al., 2017). Model precipitation during the last deglaciation (He et al., 2021) shows that Northern China and Indian monsoon affected region that can extend to SW sector here reversely correlate with the Southern China (=EC sector here), while this pattern occurs in a seesaw style, which fully supports the tripole and reversed tripole patterns of Asian monsoon rainfall behavior (Fig. 9). Moreover, variations of Haozhu cave stalagmite $\delta^{18}O$ values with supports of trace element indexes, regional peat formation (Dajiuhu peat), and additional simulation of rainfall $\delta^{18}O$ values along with annual precipitation amount (He et al., 2021), all indicate oppositely that Yangtze River tributary was wet under boreal cold or weak monsoon intensity and dry under boreal warm or strong monsoon intensity conditions (Zhang et al., 2018; He et al., 2021). In this synthesis study, we only compiled the Haozhu cave

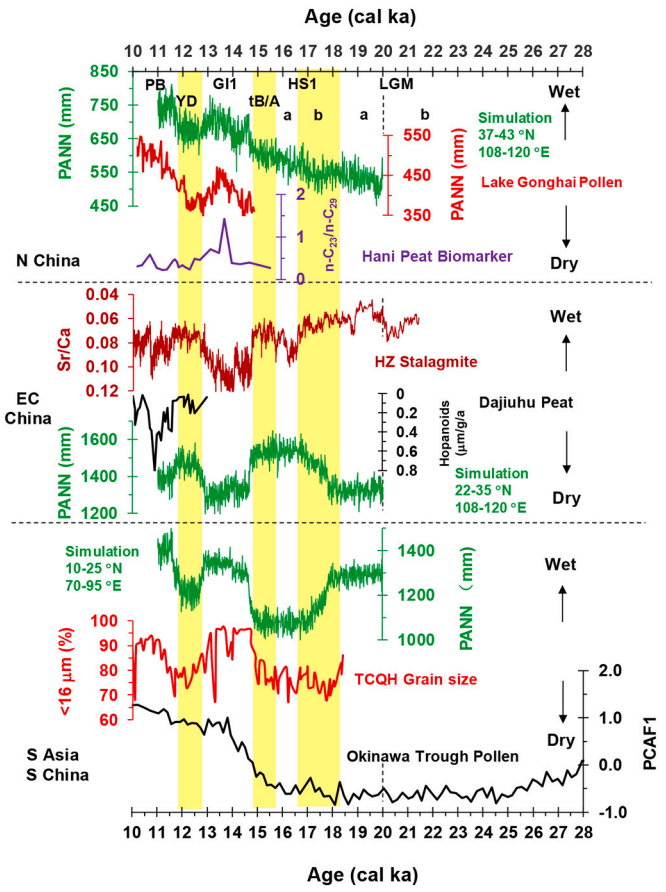

Fig. 9. Comparison of additional paleoclimate records and state-of-science model precipitation from North, East Central, and South China/South Asia showing varied Asian monsoon rainfall patterns on D-O/Heinrich-scales. The results of model precipitation in regions of 37–43°N and 108–120°E (He et al., 2021), Lake Tengchongqinghai (TCQH) grain size (Zhang et al., 2017) and Okinawa Trough pollen index (Xu et al., 2013) confirm early-stage low intensity while all records confirm late-stage profound tripole (white shade) and reversed tripole (yellow shade) patterns of Asian monsoon rainfall distribution during the boreal warm and cold interval, which is onset since 16,000 calBP. Lake Gong Hai pollen-based annual precipitation (Chen et al., 2015), Hani peat biomarker for wetness pattern (Zhou et al., 2010), Haozhu stalagmite Sr/Ca ratio (Zhang et al., 2018), Dajiuhu peat biomarker (Xie et al., 2013). State-of-science model precipitation in regions of N/S China and S Asia. It notes that high vales of biomarker in Hani and low value of biomarker flux in Dajiuhu peat, while higher percentage of finer-grained particles in the Lake TCQH reflect wetter conditions in the primary references. (For interpretation of the references to colour in this figure legend, the reader is referred to the web version of this article.)

stalagmite $\delta^{18}O$ values, selected from large numbers of Chinese stalagmite records for discussion.

Although the modeling simulation has been conducted to show that the meridional displacement of the WJS modulates the Asian monsoon rainbelt distribution during the Holocene period (Chiang et al., 2017, 2020; Kong et al., 2017), the circumglobal WJS could propagate differently during the glacial period. Given that the glacial-period ice sheet and the WJS displacement on intra D-O/Heinrich scales, we further compiled records related to climate forcing factors to explain the mechanisms for the 2-stage evolution of the Asian monsoon rainfall behaviors.

4. Discussion of the mechanism of the glacial-period Asian monsoon evolution

4.1. Background of external forcing

Increase of summer solar radiation at 23,000 calBP initiated the last deglaciation (Ullman et al., 2015a; Ullman et al., 2015b) and at 19,000 calBP accelerated the deglacial process over Northern Hemisphere (He et al., 2013). Significant rise of atmospheric CO_2 concentration at 16,000–14,000 calBP (Marcott et al., 2014) along with the highest summer solar radiation at 11,000 calBP virtually began the end of the

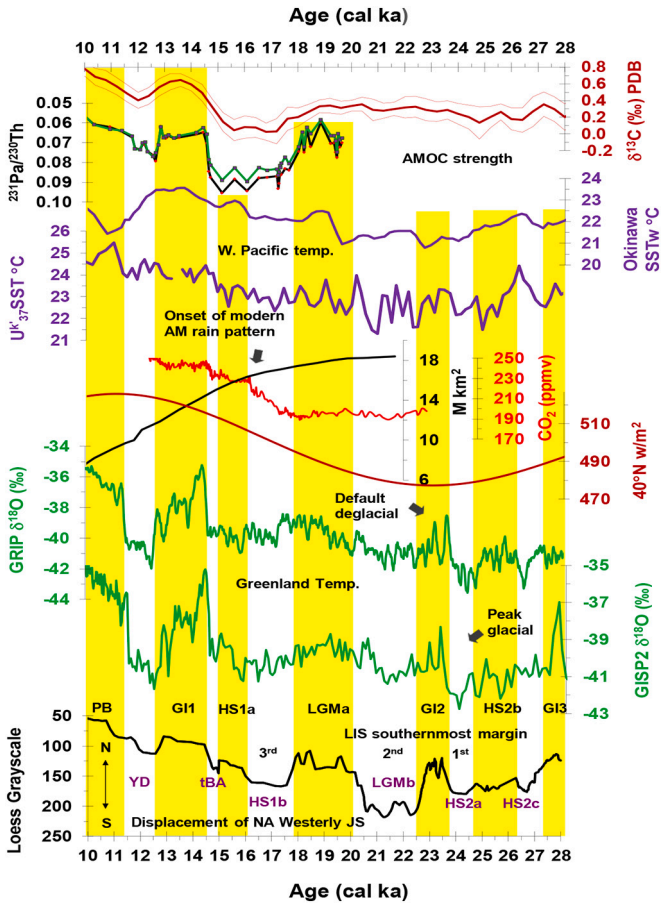

Fig. 10. a. North American WJS poleward-equatorward displacement proxy (this study); b, GISP2 record (Grootes et al., 1993); c, GRIP record (GRIP members, 1993); d, Boreal summer insolation at 40°N; e, CO_2 concentration from West Antarctic Ice Sheet Divide ice core (WIDC) (Marcott et al., 2014); f, Variation of North American Ice Sheets (Laurentide, Cordilleran, Innuitian) in million (M) km^2, which shrinks by 2 M km^2 from 22,000 to 16,000 calBP but 10 M km^2 from 16,000 to 10,000 calBP (Dalton et al., 2020); g, Average Okinawa Trough sea surface temperature (Li et al., 2001) and h, winter sea surface temperature (Liu et al., 2001) in West Pacific Ocean; i, $^{231}Pa/^{230}Th$ ratio from Bermuda as AMOC proxy (McManus et al., 2004). j, $\delta^{13}C$ values of 8 benthic foraminifera with 2 standard errors as AMOC index (Lynch-Stieglitz et al., 2014). The comparison showing that the AMOC strength lacks intra D-O/Heinrich-scale variance before the LGMa intra phase and no drastic change at about 16,000 calBP, but the poleward-equatorward displacement of the North American WJS, retreat-advance of the North American Ice Sheets, Greenland air temperature, and East China Sea surface temperature all vary in-phase with intra D-O/Heinrich-scale changes and drastic change at about 16,000 calBP. It suggests that the poleward-equatorward displacement of the North American WJS and the Laurentide Ice Sheet advance-retreat at midlatitudes and upper-midlatitudes initiated by boreal summer insolation and sudden rise of atmosphere CO_2 could be responsible for the 2-stage evolution of the Asian monsoon rainfall behavior between 28,000 and 10,000 calBP.

last glaciation (Fig. 10). The compiled North American climate stratigraphy clearly indicates that the warm GI2 phase, peaked at 23,500 calBP, represents the default deglaciation and the warm LGMa phase, peaked at 19,000 calBP, reveals the significant decay of the Laurentide Ice Sheet at southern margins, e.g. Kankakee Torrent of the meltwater flood (Figs. 1, 3). Moreover, the composite climate stratigraphy also shows that warm HS1a, GI1, and PB intervals since 16,000 calBP correspond to the accelerated warming trend as extraordinary decay of the North American Ice Sheets (Dalton et al., 2020; Fig. 10). However, although these external forcing factors ubiquitously explain the mechanisms of the abrupt climate changes over Northern Hemisphere during the last deglaciation, it has been debated what forcing mechanisms are responsible for the (intra) D-O/Heinrich-scale climatic changes. At this stage, it is also unclear what mechanisms invoke the 2-stage evolution of the Asian monsoon rainfall behavior synthesized from this research.

4.2. Mechanisms of the glacial-period Asian monsoon evolution

Fig. 10 reveals that the North Atlantic Meridional Overturning Circulation (AMOC) is unlikely the mechanism for the glacial-period 2-stage Asian monsoon evolution nor for the intra D-O/Heinrich scale climate oscillations over Northern Hemisphere on two facts: AMOC records do not show the intra D-O/Heinrich-scale variance and the substantial change during the HS1a intra phase at 16,000 calBP (McManus et al., 2004; Lynch-Stieglitz et al., 2014). It has been noted that the strong AMOC mode with little or no change is observed through the most of the last glacial period (Lynch-Stieglitz et al., 2014; Böhm et al., 2015; Kleppin et al., 2015). Modeling studies also suggest that with or without shutdown or weakened AMOC modes, Northern Hemisphere D—O cyclic temperature changes would still persist over the Greenland and Atlantic basin (Seager et al., 2002). On the other hand, poleward-equatorward displacements of the North American WJS, the Laurentide Ice Sheet advance-retreat at its southernmost margins, the Greenland temperature variation (Grootes et al., 1993; GRIP members, 1993), and the poleward-equatorward displacement of West Pacific Warm Pool (= ITCZ; Xu et al., 2013; Liu et al., 2001; Li et al., 2001) all vary on intra D-O/Heinrich scales with an extraordinarily change at 16,000 calBP (Fig. 10). We propose that the poleward-equatorward displacement of the North American WJS and retreat-advance of the Laurentide Ice Sheet southernmost margins, which superposes on slow and profoundly fast ice sheet decay modes, controlled the boreal intra D-O/Heinrich-scale climate changes and the 2-stage evolution of the Asian monsoon rainfall behavior.

4.3. Combination of glacial-period and modern WJS forcing theories

Fluctuations of North American Ice Sheets cause the Intertropical Convergence Zone (ITCZ) migration and contraction/expansion (Chiang and Bitz, 2005). The enlargement and reduction of North American Ice Sheets (Dalton et al., 2020) and associated sea ice coverage increased and decreased the Northern Hemisphere albedo and reduced and increased UV absorption (Li et al., 2005b). Moreover, fluctuations of North American Ice Sheets during the last deglacial period could have frequently reorganized the atmospheric pressure system that largely modulated the structure and intensity of the WJS circulation (Chiang and Bitz, 2005; Wunsch, 2006; Wassenburg et al., 2016). Importantly, southernly- and northernly-bulged and/or migrated North American WJS over varied size and thickness of the Laurentide Ice Sheet (Wunsch, 2006) would have quickly propagated over Northern Hemisphere, enhancing the North American-Asian atmospheric teleconnection (Clark et al., 1999).

Modern atmospheric theories suggest that the subtropical WJS carries moisture from low level jet or Atmospheric River (although it can migrate by itself) and high-level Hadley Cell to migrate from the tropical Indian and subtropical West Pacific Oceans to midlatitudes, and the polar front WJS carries cold airmass from the subarctic to midlatitudes via meandering Rossby waves (Uccellini and Johnson, 1979; Boers et al., 2019). At the place where Asian subtropical and polar front WJS merges, Asian monsoon rainbelts occur (Yeh et al., 1959; Lau and Li, 1984; Lin and Lu, 2005; Li et al., 2005a; Sampe and Xie, 2010). Three types of merges could cause different intensity of monsoon rainfall events: 1) the southernly-bulged polar front jet superposes on the water-laden flat subtropical jet stream to form intense rainfall events; 2) the northernly-bulged subtropical jet superposes on the flat polar front jet stream to form somewhat strong rainbelt; and 3) oppositely-bulged polar front and subtropical jet streams superpose each other to form local-scale rains (Berggren et al., 1949; Rex, 1950a, 1950b; Li and Wang, 2003; Woollings et al., 2010; Handlod and Martin, 2016; Winters and Martin, 2017). These changes could well be regulated by the changing atmospheric pressure system, e.g. changes from positive to negative Arctic Oscillation or North Atlantic Oscillation mode or vice versa (Handlod and Martin, 2016; Winters and Martin, 2017).

4.4. Synthesis of the potential mechanism for the glacial-period Asian monsoon evolution

For synthesizing the stage 1 mechanism between 28,000 and 18,000 calBP, the large North American Ice Sheets, indicated by fluctuations of Laurentide Ice Sheet southernmost margins at as low as 39–42°N (Dalton et al., 2020), functioned as a mechanic barrier splitting the WJS into south and north branches (Kutzbach and Wright Jr., 1985; Manabe and Broccoli, 1985). The resultant high-pressure system (anticyclones) could expand from upper-midlatitudes to midlatitudes, forcing the low-pressure system (cyclones) wander far south of the ice sheet margins (Bromwich et al., 2004, 2005), forming a positive Arctic Oscillation mode in summers (Fig. 11a). The North American WJS could propagate quickly to the Eurasian continent, steering Rossby waves causing rainbelts distribution in certain ways. For relative wet EC and dry NE/SW sectors of China from warm GI3 to relatively cold HS2 intra phases (Figs. 8, 9), a strong anticyclone system as a blocking high cell could displace a stationary ridge of the subtropical WJS to 40°N, stagnating summer monsoon rainbelts over the Yangtze River tributary with little rainfall in NE/SW China (see Fig. 11a). For relatively high monsoon rainfall pulses in NE/SW sectors from warm GI2 to relatively cold LGM phases (Figs. 8, 9), a mixture of intermittently strong and weak anticyclone system, functioning as a weaker blocking cell, could displace transient ridges of the subtropical WJS northward to 45°N into NE sectors of China, which could allow low level jet streams from the tropical Indian Ocean migrate to SW China (An et al., 2011; Hong et al., 2018; see Fig. 11b). We expect that southernly-bulged polar front jet streams and northernly-bulged subtropical jet streams merged from place to place, causing low intensity of Indian and East Asian monsoon rains during the Asian monsoon evolution stage 1, when blocking high cell systems prevail over midlatitudes and warm surface waters in the tropical and subtropical Indian and West Pacific Oceans drift away from Asian coasts (Xu et al., 2013).

For synthesizing the stage 2 mechanism between 18,000 and 10,000 calBP, the decayed North American Ice Sheets, indicated by fluctuations of the Laurentide Ice Sheet southern margins at north of 45°N especially after 16,500 calBP, the Laurentide Ice Sheet as the mechanic barrier for the WJS poleward displacement was no longer effective. Importantly, North American Ice Sheets shrank by 10 million km^2 from 16,000 to 10,000 calBP comparing with only 2 million km^2 from 22,000 to 16,000 calBP (Dalton et al., 2020; Fig. 10), which allowed the North American subtropical WJS displace increasingly poleward (Wang et al., 2012; also see Bromwich et al., 2004, 2005; Figs. 10, 11b). The resultant ITCZ poleward migration/expansion became intensified, and the subtropical and polar front WJS could more frequently merge to produce large-scale rainbelts over areas previously covered by the Laurentide Ice Sheet (Fig. 11b). This resulted in low-pressure cyclones extending from the subtropical to midlatitude regions, forcing high-pressure anticyclones wandering progressively over upper-midlatitudes to produce a negative

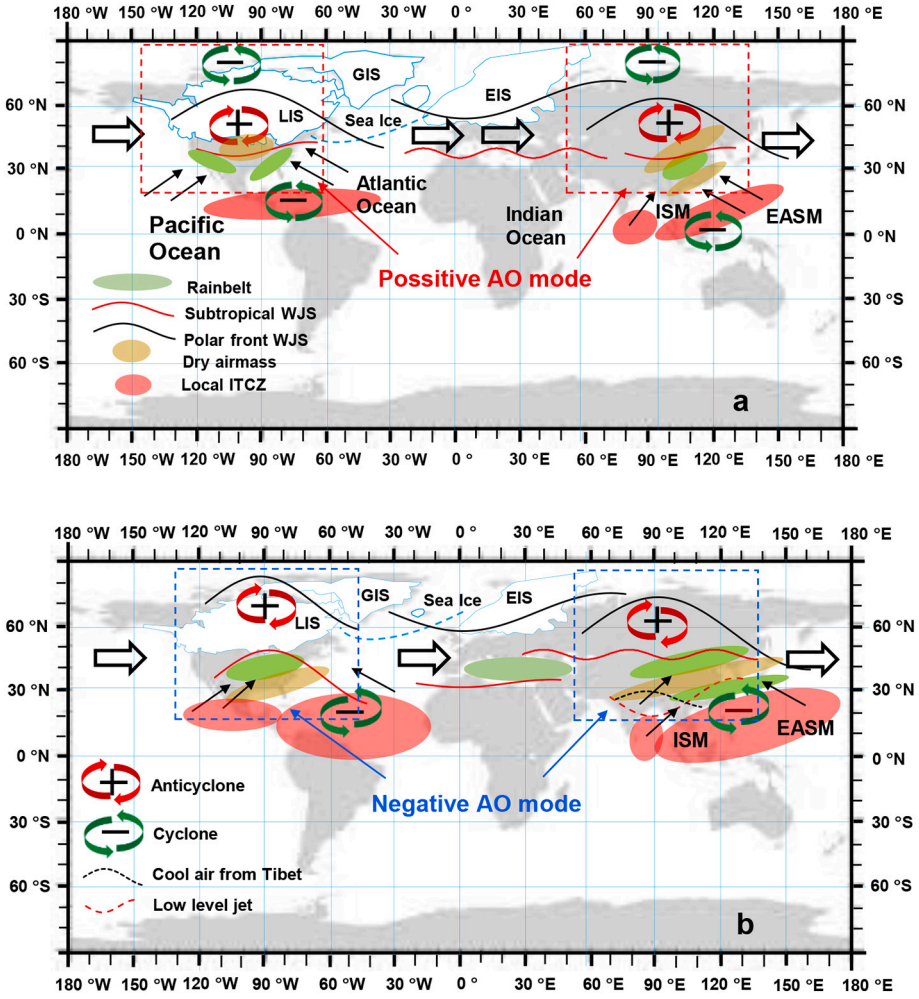

Fig. 11. Schematic diagrams summarizing synthesized models of the North American WJS forcing on paleoclimate changes on intra D-O/Heinrich scales over Northern Hemisphere. **a**. Under large North American Ice Sheets and sea ice coverage (e.g. before 16,000 calBP), LIS advance, and ITCZ contraction scenario, the North American WJS equatorward displacement produces positive Arctic Oscillation mode in summers, separated polar front and subtropical WJSs stagnate rainbelts far south of LIS margins, merged East Asian polar front and subtropical WJSs at 40°N steer Asian monsoon rainbelts over EC sector leaving NE/SW and surrounding areas of China dry (reversed tripole monsoon rainfall mode). **b**. Under smaller North American Ice Sheets and sea ice coverage, LIS retreat, and ITCZ expansion scenario, the poleward displacement of the North American WJS produces negative Arctic Oscillation mode in summers, merged polar front and subtropical WJSs move rainbelt closer to LIS margins, merged East Asian polar front and subtropical WJSs at 45°N steers heavy monsoon rainfall over NE leaving little precipitation over EC China, and merged low level jet (Atmospheric River) from the Indian and East Asian Summer Monsoon circulation with cool air flow from the Tibet causes rain events over SW and surrounding areas of China (tripole monsoon rainfall mode). LIS: Laurentide Ice Sheet; GIS: Greenland Ice Sheet; EIS: Eurasia Ice Sheet; ISM: Indian Summer Monsoon; EASM: East Asian Summer Monsoon.

Arctic Oscillation mode in summers (Fig. 11b). The North American WJS could propagate quickly to the Eurasian continent steering Rossby waves, causing rainbelts distribution in certain ways. For the tripole monsoon rainfall pattern during warm GI1 and PB intervals (Figs. 8, 11b), a strong cyclone system over large areas of midlatitudes could allow the subtropical WJS to develop a stationary flat trough, wandering semi-permanently at 45°N, stretching the heavy East Asian Summer Monsoon rainbelt over NE sector and surrounding North China sectors (Figs. 8, 9, 11b). Atmospheric Rivers displaced northward from expanded warm ocean pools, merging with the sunken cool air parcel, slid from the Tibet Plateau, causing heavy Indian Summer Monsoon rainfall in SW and surrounding South China sectors (Figs. 8, 9, 11b). At the same time, the Yangtze River tributary and surrounding EC China sectors received relatively low monsoon precipitation (Figs. 8, 9, 11b). For reversed tripole rainfall patterns during relatively cold boreal HS1 and YD intervals, a weak cyclone system over midlatitudes could allow the subtropical WJS to develop a stationary trough displacing poleward semi-permanently at 40°N (see Fig. 11a), causing the Yangtze River tributary to receive intense monsoon rains but leaving over NE/SW China dry (Figs. 8, 9, 11a). After 16,000 calBP, the overall intensity of Asian monsoon rainfall reached to the summit from place to place. We expect that deep troughs and ridges of the polar front WJS merged with the massive water-laden subtropical WJS for heavy rainfall events due to accelerated deglacial process over Northern Hemisphere, increasing atmospheric CO_2 and air temperature, poleward migrated/expanded ITCZ, and poleward shifting of warm pools from the tropical Indian and subtropical West Pacific Oceans to the East China Sea (Xu et al., 2013; Fig. 10).

In sum, the poleward-equatorward displacement of the North American WJS and associated retreat-advance of the Laurentide Ice Sheet from midlatitudes to upper-midlatitudes are responsible for the 2-stage evolution of the Asian monsoon rainfall behavior with intra D-O/Heinrich scale variabilities. Before and after 18,000 calBP, the Laurentide Ice Sheet southern margins fluctuated at midlatitudes with influence of ice sheet geometry and at upper midlatitudes without much influence of its geometric on boreal WJS propagations (Wang et al., 2012), which was triggered and accelerated by the boreal solar radiation and rising of atmospheric CO_2 concentration.

5. Conclusion

In the central USA, places along retreating Laurentide Ice Sheet southernmost margins, 13 intra D-O/Heinrich scale climate stratigraphic units were synthesized from loess, dune, lacustrine, and glacial moraine geomorphological successions between 28,000 and 10,000 calBP. This synthesized climate stratigraphy highlights: 1) the Laurentide Ice Sheet advanced to the southernmost margin during the HS2a phase, defined as the peak glacial; 2) the GI2 interstadial represents the first-time ice margin retreat since the peak glacial, defined as the default deglaciation; 3) the Laurentide Ice Sheet advanced to the second southernmost (several) margins during the LGMb phase; 4) the Laurentide Ice Sheet advanced to the third southernmost margin during the HS1b phase in Illinois, USA and then on its way toward the polar region. These fast-pacing climate changes superpose on a 2-stage North American ice sheets decay trend: in the first 6000 years from 22,000 to 16,000 calBP total ice sheet areas reduces by 2 million km^2 and in the second

6000 years from 16,000 to 10,000 calBP total ice sheet areas reduces by 10 million km^2. The significance of the North American composite climate stratigraphy is synthesized as a proxy to represent advance-retreat of the Laurentide Ice Sheet southern margins and the poleward-equatorward displacement of the North American WJS.

In China, 2-stage evolution of Asian monsoon rainfall modes were synthesized from the compilation of lacustrine organic carbon content record over NE, stalagmite $\delta^{18}O$ record over EC, and lacustrine cellulose $\delta^{13}C$ record over SW sectors all with reliable chronologies between 28,000 and 10,000 calBP. During the stage 1 between 28,000 and 18,000 calBP, Asian monsoon rainfall intensity firstly decreased over NE/SW but increased over EC, and then substantially fluctuated between strong and weak over NE/SW sectors and remained constant over EC sector. During the stage 2 between 18,000 and 10,000 calBP, Asian monsoon rainbelts distributed a profound tripole mode during boreal warm and a reversed-tripole mode during boreal cold intervals, resembling modern synoptic weather system over East Asia, which came onset at about 16,000 calBP. Findings are further corroborated by 6 additional classical paleoclimate records with reliable chronology but shorter sequences and 3 state-of-the-science model precipitation records from 20,000 to 11,000 calBP in N/S China and South Asia. The poleward-equatorward displacement of the North American tropospheric WJS and associated Laurentide Ice Sheet advance-retreat in midlatitudes or upper midlatitudes were summarized to modulate the 2-stage evolution of the Asian monsoon rainfall behavior via the North American-Asian atmospheric teleconnection. Synthesized models from compilation of hypothesis/theories of glacial-period and modern atmospheric circulation forcing factors summarize the mechanisms in details to explain the 2-stage evolution of the Asian monsoon rainfall behaviors.

Declaration of Competing Interest

This paper has not been published and is not considered for publication elsewhere. All authors have made substantial contributions to this compilation/synthesis/discussion article. We declare that this research has no Conflict of Interest and any Ethical Issues. The detail of individual contributions of each co-author to the article has listed in the cover page, and we confirm that all authors have approved the final version of the manuscript.

Acknowledgement

This research was partially supported by the Strategic Priority Research Program of Chinese Academy of Sciences (Grant no. XDB40010200), International Partnership Program of Chinese Academy of Sciences (Grant No. 132B61KYSB20170005), and the Open-end Fund Program of State Key Laboratory of Loess and Quaternary Geology, Institute of Earth Environment, Chinese Academy of Sciences (Grant no. SKLLQG1853). We also thank Drs. Leon Follmer, Don McKay, and Andy Stumpf for valuable comments and for one anonymous reviewer for helpful reviews and suggestions.

References

GRIP members, 1993. Climate instability during the last interglacial period recorded in the GRIP ice core. Nature 364, 203–207.

Dalton, et al., 2020. An updated radiocarbon-based ice margin chronology for the last deglaciation of the North American Ice Sheet Complex. Quat. Sci. Rev. 234, 106223. https://doi.org/10.1016/j.quascirev.2020.106223.

An, Z.S., Clemens, S.C., Shen, J., Qiang, X., Jin, Z., Sun, Y., Prell, W.L., Luo, J., Wang, S., Xu, H., Cai, Y., Zhou, W., Liu, X., Liu, W., Shi, Z., Yan, L., Xiao, X., Chang, H., Wu, F., Ai, L., Lu, F., 2011. Glacial-interglacial indian summer monsoon dynamics. Science 333, 719–723.

Asmerom, Y., Polyak, V.J., Burns, S.J., 2010. Variable winter moisture in the southwestern United States linked to rapid glacial climate shifts. Nat. Geosci. 3, 114–117.

Berggren, R., Bolin, B., Rossby, C.G., 1949. An aerological study of zonal motion, its perturbations and break-down. Tellus 1, 14–37.

Boers, N., Goswami, B., Rheinwalt, A., Bookhagen, B., Hoskins, B., Kurths, J., 2019. Complex networks reveal global pattern of extreme-rainfall teleconnections. Nature 566, 373–377.

Böhm, E., et al., 2015. Strong and deep Atlantic meridional overturning circulation during the last glacial cycle. Nature 517, 73–76.

Broecker, W., Bond, G., Klas, M., Clark, E., McManus, J., 1992. Origin of the northern Atlantic's Heinrich events. Clim. Dyn. 6, 265–273.

Bromwich, D.H., Toracinta, E.R., Wei, H., Oglesby, R.J., Fastook, J.L., Hughes, T.J., 2004. Polar MM5 simulations of the winter climate of the Laurentide Ice Sheet at the LGM. J. Clim. 17, 3415–3433.

Bromwich, D.H., Toracinta, E.R., Oglesby, H., Fastook, J.L., Hughes, T.J., 2005. LGM summer climate on the Southern margin of the Laurentide ice sheet: wet or dry? J. Clim. 18, 3317–3338.

Campbell, M.C., Fisher, T.G., Goble, R.J., 2011. Terrestrial sensitivity to abrupt cooling recorded by aeolian activity in northwest Ohio, USA. Quat. Res. 75, 411–416.

Chen, F., Xu, Q., Chen, J., Birks, H.J.B., Liu, J., Zhang, S., Jin, L., An, C., Telford, R.J., Cao, X., 2015. East Asian summer monsoon precipitation variability since the last deglaciation. Sci. Rep. 5, 11186. https://doi.org/10.1038/srep11186.

Cheng, H., Edwards, R.L., Sinha, A., Spotl, C., Yi, L., Chen, S., Kelly, M.J., Kathayat, G., Wang, X., Li, X., 2016. The Asian monsoon over the past 640,000 years and ice age terminations. Nature 534, 640–646.

Cheng, H., Zhang, H., Zhao, J., Li, H., Ning, Y., Kathayat, G., 2019. Chinese stalagmite paleoclimate researches: a review and perspective. Sci. China Earth Sci. 62, 1489–1513.

Chiang, J.C.H., Bitz, C.M., 2005. Influence of high latitude ice cover on the marine Intertropical Convergence Zone. Clim. Dyn. 25, 477–496.

Chiang, J.C.H., Swenson, L.M., Kong, W., 2017. Role of seasonal transitions and the westerlies in the interannual variability of the East Asian summer monsoon precipitation. Geophys. Res. Lett. 44, 3788–3795.

Chiang, J.C.H., Herman, M.J., Yoshimura, K., Fung, I.Y., 2020. Enriched East Asian oxygen isotope of precipitation indicates reduced summer seasonality in regional climate and westerlies. PNAS 117, 14745–14750. www.pnas.org/cgi/doi/10.1073/pnas.1922602117.

Clark, P.U., Alley, R.B., Pollard, D., 1999. Climatology - Northern hemisphere ice-sheet influences on global climate change. Science 286, 1104–1111.

Clemens, S.C., Prell, W.L., Sun, Y.B., 2010. Orbital-scale timing and mechanisms driving Late Pleistocene Indo-Asian summer monsoons: reinterpreting cave speleothem $\delta^{18}O$. Paleoceanography 25, PA4207. https://doi.org/10.1029/2010PA001926.

Cressman, G.P., 1981. Circulations of the West Pacific jet stream. Mon. Weather Rev. 109, 2450–2463.

Curry, B.B., Grimm, E.C., Slate, J.E., Hansen, B.C., Konen, M.E., 2007. The Late Glacial and Early Holocene Geology, Paleoecology, and Paleohydrology of the Brewster Creek Site, a Proposed Wetland Restoration Site, Pratt's Wayne Woods Forest Preserve and James "Pate" Philip State Park, Bartlett, Illinois. Illinois State Geological Survey, Champaign. Circular 571.

Curry, B.B., Hajic, E.R., Clark, J.A., Befus, K.M., Carrell, J.E., Brown, S.E., 2014. The Kankakee Torrent and other large meltwater flooding events during the last deglaciation, Illinois, USA. Quat. Sci. Rev. 90, 22–36.

Curry, B.B., Lowell, T.V., Wang, H., Anderson, A.C., 2018. Revised time-distance diagram for the Lake Michigan Lobe, Michigan Subepisode, Wisconsin Episode, Illinois, USA. Geol. Soc. Am. Spec. Pap. 530, 69–101.

Dayem, K.E., Molnar, P., Battisti, D.S., Roe, G.H., 2010. Lessons learned from oxygen isotopes in modern precipitation applied to interpretation of speleothem records of paleoclimate from eastern Asia. Earth Planet Sci. Lett. 295, 219–230.

Ding, Y.H., Wang, Z.Y., Sun, Y., 2008. Inter-decadal variation of the summer precipitation in East China and its association with decreasing Asian summer monsoon. Part I: observed evidences. Int. J. Climatol. 28, 1139–1161.

Ding, Y.H., Sun, Y., Wang, Z.Y., Zhu, Y.X., Song, Y.F., 2009. Inter-decadal variation of the summer precipitation in China and its association with decreasing Asian summer monsoon Part II: possible causes. Int. J. Climatol. 29, 1926–1944.

Dorale, J.A., Wozniak, L.A., Bettis III, E.A., Carpenter, S.J., Mandel, R.D., Hajic, E.R., Lopinot, N.H., Ray, J.H., 2010. Isotopic evidence for Younger Dryas aridity in the North American midcontinent. Geology 38, 519–522.

Follmer, L.R., McKay, D.E., Lineback, J.A., Gross, D.L., Wisconsinan, Sangamonian, 1979. Illinoian stratigraphy in central Illinois: Illinois State Geological Survey Guidebook, 13, pp. 19–21.

Frye, J.C., Willman, H.B., 1960. Classification of the Wisconsinan Stage in the Lake Michigan Glacial Lobe: Illinois State Geological Survey Circular, vol. 285 (16 p).

Frye, J.C., Willman, H.B., 1973. Wisconsinan climatic history interpreted from Lake Michigan Lobe deposits and soils. In: Black, R.F., Goldthwait, R.P., Willman, H.B. (Eds.), The Wisconsin Stage: Geological Society of America Memoir, 136, pp. 135–152. https://doi.org/10.1130/MEM136-p135.

Grimm, E.C., Wattsb, W.A., Jacobson Jr., G.L., Hansend, B.C.S., Almquiste, H.R., Dieffenbacher-Krallc, A.C., 2006. Evidence for warm wet Heinrich events in Florida. Quat. Sci. Rev. 25, 2197–2211.

Grootes, P.M., Stuiver, M., White, J.W.C., Johnsen, S., Jouzel, J., 1993. Comparison of Oxygen-Isotope Records from the Gisp2 and Grip Greenland Ice Cores. Nature 366, 552–554.

Handlod, Z.J., Martin, J.E., 2016. Composit analysis of large-scale environments conductive to Western Pacific polar/subtropical jet superposition. J. Clim. 29, 7145–7165.

Hansel, A.K., Johnson, W.H., 1986. Late Quaternary record of the Chicago Outlet area. In: Hansel, A.K., Johnson, W.H. (Eds.), Quaternary Records of Northeastern Illinois and Northwestern Indiana: Illinois State Geological Survey Guidebook, vol. 22, pp. 61–72.

Hansel, A.K., Johnson, W.H., 1992. Fluctuations of the Lake Michigan Lobe during the late Wisconsin Subepisode: Sveriges Geologiska Undersökning, 81, pp. 133–144.
Hansel, A.K., Johnson, W.H., 1996. Wedron and Mason groups: Lithostratigraphic Reclassifi cation of deposits of the Wisconsin Episode. In: Lake Michigan Lobe Area: Illinois State Geological Survey Bulletin, 104, p. 116.
Hansel, A.K., Mickelson, D.M., 1988. A reevaluation of the timing and causes of high lake phases in the Lake Michigan Basin. Quat. Res. 29, 113–128. https://doi.org/10.1016/0033-5894(88)90055-5.
He, F., Shakun, J.D., Clark, P.U., Carlson, A.E., Liu, Z.Y., Otto-Bliesner, B.L., Kutzbach, J. E., 2013. Northern Hemisphere forcing of southern Hemisphere climae during the last deglaciation. Nature 494, 81–85.
He, C., Liu, Z., Otto-Bliesner, B.L., Brady, E.C., Zhu, C., Tomas, R., Clark, P.U., Zhu, J., Jahn, A., Gu, S., Zhang, J., Nusbaumer, J., Noone, D., Cheng, H., Wang, Y., Yan, M., Bao, Y., 2021. Hydroclimate footprint of pan-Asian monsoon water isotope during the last deglaciation. Sci. Adv. 7, eabe2611.
Heath, S.L., Loope, H.M., Curry, B.B., Lowell, T.V., 2018. Pattern of southern Laurentide Ice Sheet margin position changes during Heinrich Stadials 2 and 1. Quat. Sci. Rev. 201, 362–379.
Hong, B., Uchida, M., Hong, Y., Peng, H., Kondo, M., Ding, H., 2018. The respective characteristics of millennial-scale changes of the India summer monsoon in the Holocene and the Last Glacial. Palaeogeogr. Palaeoclimatol. Palaeoecol. 496, 155–165.
Hou, J., Huang, Y., Wang, Y., Shuman, B., Oswald, W.W., Faison, E., Foster, D.R., 2006. Postglacial climate reconstruction based on compoundspecific D/H ratios of fatty acids from Blood Pond, New England. Geochem. Geophys. Geosyst. 7, Q03008 https://doi.org/10.1029/2005GC001076.
Johnson, K.R., Hu, C.Y., Belshaw, N.S., Henderson, G.M., 2006. Seasonal trace-element and stable-isotope variations in a Chinese speleothem: the potential for high-resolution paleomonsoon reconstruction. Earth Planet Sci. Lett. 244, 394–407.
Kleppin, H., Jochum, M., Otto-Bliesner, B., Shields, C.A., Yeager, S., 2015. Stochastic atmospheric forcing as a cause of Greenland Climate Transition. J. Clim. 28, 7741–7763.
Kong, W.W., Swenson, L.M., Chiang, J.C.H., 2017. Seasonal Transitions and the Westerly Jet in the Holocene East Asian Summer Monsoon. J. Clim. 30, 3343–3365.
Kutzbach, J.E., Wright Jr., H.E., 1985. Simulation of the climate of 18,000 yr BP: results for the North American/North Atlantic/European sector. Quat. Sci. Rev. 4, 147–187.
Lambert, W.J., Aharon, P., Hellstrom, J., 2010. The Response of Extratropical Westerlies to Climate Change (31.9-11.3 ka) Revealed by a Speleothem from DeSoto Caverns, Alabama (USA). AGU 2010 San Francisco Annual Meeting 12/13/2010- 12/17/2010.
Lau, K.M., Li, M.T., 1984. The monsoon of East-Asia and its global associations - a survey. B. Am. Meteorol. Soc. 65, 114–125.
Li, J.P., Wang, J.L.X.L., 2003. A modified zonal index and its physical sense. Geophys. Res. Lett. 30. https://doi.org/10.1029/2003GL017441.
Li, T.G., Liu, Z.X., Hall, M.A., Berne, S., Saito, Y., Cang, S.X., Cheng, Z.B., 2001. Heinrich event imprints in the Okinawa Trough: evidence from oxygen isotope and planktonic foraminifera. Palaeogeogr. Palaeoclimatol. Palaeoecol. 176, 133–146.
Li, J., Yu, R.C., Zhou, T.C., Wang, B., 2005a. Why is there an early spring cooling shift downstream of the Tibetan Plateau? J. Clim. 18, 4660–4668.
Li, C., Battisti, D.S., Schrag, D.P., Tziperman, E., 2005b. Abrupt climate shifts in Greenland due to displacements of the sea ice edge. Geophys. Res. Lett. 32, L19702 https://doi.org/10.1029/2005GL023492.
Liang, X.Z., Wang, W.C., 1998. Associations between China monsoon rainfall and tropospheric jets. Quart. J. R. Meteorol. Soc. 124, 2597–2623.
Lin, Z.D., Lu, R.Y., 2005. Interannual meridional displacement of the east Asian upper-tropospheric jet stream in summer. Adv. Atmos. Sci. 22, 199–211.
Liu, Z.X., et al., 2001. The paleoclimatic events and cause in the Okinawa Trough during 50 kaBP. Chin. Sci. Bull. 46, 153–157.
Liu, J., Chen, J., Zhang, X., Li, Y., Rao, Z., Chen, F., 2015. Holocene East Asian summer monsoon records in northern China and their inconsistency with Chinese stalagmite δ18O records. Earth Sci. Rev. 148, 194–208.
Lowell, T.V., Hayward, R.K., Denton, G.H., 1999. Role of climate oscillations in determining ice-margin position: Hypothesis, examples, and implications. Geol. Soc. Am. Spec. Pap. 337, 193–203.
Xu, D.K., Lu, H.Y., Wu, N.Q., Liu, Z.X., Li, T.G., Shen, C.M., Wang, L., 2013. Asynchronous marine-terrestrial signals of the last deglacial warming in East Asia associated with low- and high-latitude climate changes. PNAS 110, 9657–9662.
Lynch-Stieglitz, J., Schmidt, M.W., Henry, L.G., Curry, W.B., Skinner, L.C., Mulitza, S., Zhang, R., Chang, P., 2014. Muted change in Atlantic overturning circulation over some glacial-aged Heinrich events. Nat. Geosci. 7, 144–150.
Manabe, S., Broccoli, A.J., 1985. The influence of continental ice sheets on the climate of an ice age. J. Geophys. Res. 90, 2167–2190.
Marcott, S.A., Bauska, T.K., Buizert, C., Steig, E.J., Rosen, J.L., Cuffey, K.M., Fudge, T.J., Severinghaus, J.P., Ahn, J., Kalk, M.L., McConnell, J.R., Sowers, T., Taylor, K.C., White, J.W.C., Brook, E.J., 2014. Centennial-scale changes in the global carbon cycle during the last deglaciation. Nature 514, 616–619.
Mason, J.A., Miao, X., Hanson, P.R., Johnson, W.C., Jacobs, P.M., Goble, R.J., 2008. Loess record of the Pleistocene-Holocene transition on the northern and central Great Plains, USA. Quat. Sci. Rev. 27, 1772–1783.
McManus, J.F., Francois, R., Gherardi, J.M., Keigwin, L.D., Brown-Leger, S., 2004. Collapse and rapid resumption of Atlantic meridional circulation linked to deglacial climate changes. Nature 428, 834–837.
Miao, X., Hanson, P.R., Wang, H., Young, A.R., 2010. Timing and origin for sand dunes in the Green River Lowland of Illinois, upper Mississippi River Valley, USA. Quat. Sci. Rev. 29, 763–773.
Mingram, J., Stebich, M., Schettler, G., Hu, Y., Rioual, P., Nowaczyk, N., Dulski, P., You, H., Opitz, S., Liu, Q., Liu, J., 2018. Millennial-scale East Asian monsoon variability of the last glacial deduced from annually laminated sediments from Lake Sihailongwan, N.E. China. Quat. Sci. Rev. 201, 57–76.
Muhs, D.R., Bettis III, E.A., Aleinikoff, J.N., McGeehin, J.P., Beann, J., Skipp, G., Marshall, B.D., Roberts, H.M., Johnson, W.C., Benton, R., 2008. Origin and paleoclimatic significance of late Quaternary loess in Nebraska: evidence from stratigraphy, chronology, sedimentology, and geochemistry. Geol. Soc. Am. Bull. 120, 1378–1407.
Musgrove, M.L., Banner, J.L., Mack, L.E., Combs, D.M., James, E.W., Cheng, H., Edwards, R.L., 2001. Geochronology of late Pleistocene to Holocene speleothems from Central Texas: implications for regional paleoclimate. GSA Bull. 113, 1532–1543.
Nakamura, N., Huang, C.S.Y., 2018. Atmospheric blocking as a traffic jam in the jet stream. Science 361, 42–47.
Oster, J.L., Ibarra, D.E., Winnick, M.J., Maher, K., 2015. Steering of westerly storms over western North America at the last Glacial Maximum. Nat. Geosci. 8, 201–205.
Peteet, D.M., Daniels, R.A., Heusser, L.E., Vogel, J.S., Southon, J.R., Nelson, D.E., 1993. Late-glacial pollen, macrofossils and fish remains in northeastern U.S.A. e the Younger Dryas oscillation. Quat. Sci. Rev. 12, 597–612.
Curry, B.B., Petras, J., 2011. Lake Michigan lobe of the Laurentide Ice Sheet fro ice-walled lake deposits. Chronological framework for the deglaciation of the Lake Michigan lobe of the Laurentide Ice Sheet from ice-walled lake deposits. J. Quat Sci 26, 402–410.
Putnam, A.E., 2015. A glacial zephyr. Nat. Geosci. 8, 175–176.
Quade, J., Forester, R.M., Pratt, W.L., Carter, C., 1998. Black mats, spring-fed streams, and late-glacial-age recharge in the southern Great basin. Quat. Res. 49, 129–148.
Ramage, C.S., 1971. Monsoon Meteorology. In: International Geophysics Series, 15. Academic Press, p. 300.
Reimer, P.J., Bard, E., Bayliss, A., Beck, J.W., Blackwell, P.G., Bronk Ramsey, C., Buck, C. E., Cheng, H., Edwards, R.L., Friedrich, M., Grootes, P.M., Guilderson, T.P., Haflidason, H., Hajdas, I., Hatté, C., Heaton, T.J., Hogg, A.G., Hughen, K.A., Kaiser, K.F., Kromer, B., Manning, S.W., Niu, M., Reimer, R.W., Richards, D.A., Scott, E.M., Southon, J.R., Turney, C.S.M., van der Plicht, J., 2013. IntCal13 and MARINE13 radiocarbon age calibration curves 0–50000 years cal BP. Radiocarbon 55, 1869–1887. https://doi.org/10.2458/azu_js_rc.55.16947.
Reiter, E.R., 1963. Jet-stream Meteorology. University of Chicago Press, p. 515.
Ren, X.J., Yang, X.Q., Chu, C.J., 2010. Seasonal variations of the synoptic-scale transient Eddy activity and Polar Front Jet over East Asia. J. Clim. 23, 3222–3233.
Ren, X.J., Yang, X.Q., Zhou, T.J., Fang, J.B., 2011. Diagnostic comparison of wintertime east asian subtropical jet and polar-front jet: large-scale characteristics and transient Eddy activities. Acta Meteorol. Sin. 25, 21–33.
Rex, D.F., 1950a. Blocking action in the middle troposphere and its effect upon regional climate. I. An aerological study of blocking action. Tellus 2, 196–211.
Rex, D.F., 1950b. Blocking action in the middle troposphere and its effect upon regional climate. II. The climatology of blocking action. Tellus 2, 275–301.
Sampe, T., Xie, S., 2010. Large-scale dynamics of the Meiyu-Baiu Rainband: environmental forcing by the Westerly Jet. J. Clim. 23, 113–134.
Seager, R., Battisti, D.S., Yin, J., Gordon, N., Naik, N., Clement, A.C., Cane, M.A., 2002. Is the Gulf Stream responsible for Europe's mild winters? Quat. J. R. Meteorol. Soc. 128, 2563–2586.
Strong, C., Davis, R.E., 2008. Variability in the position and strength of winter jet stream cores related to northern hemisphere teleconnections. J. Clim. 21, 584–592.
Trenberth, K.E., Guillemot, C.J., 1996. Physical processes involved in the 1988 drought and 1993 floods in North America. J. Clim. 9, 1288–1298.
Uccellini, L.W., Johnson, D.R., 1979. Coupling of upper and lower tropospheric jet streaks and implications for the development of severe convective storms. Mon. Weather Rev. 107, 682–703.
Ullman, D.J., et al., 2015a. Southern Laurentide ice-sheet retreat synchronous with rising boreal summer insolation. Geology 43, 23–26.
Ullman, D.J., Carlson, A.E., Anslow, F.S., LeGrande, A.N., Licciardi, J.M., 2015b. Laurentide ice-sheet instability during the last deglaciation. Nat. Geosci. 8, 534–U140.
Wagner, J.D.M., Cole, J.E., Beck, J.W., Patchett, P.J., Henderson, G.M., Barnett, H.R., 2010. Moisture variability in the southwestern United States linked to abrupt glacial climate change. Nat. Geosci. 3, 110–113.
Wang, H., Follmer, L.R., Liu, J.C., 2000. Isotope evidence of paleo-El Niño-Southern Oscillation cycles in loess-paleosol record in the Central United States. Geology 28, 771–774.
Wang, Y.J., Cheng, H., Edwards, R.L., An, Z., Wu, J., Shen, C.-C., Dorale, J.A., 2001. A high-resolution absolute-dated late Pleistocene monsoon record from Hulu Cave, China. Science 294, 2345–2348.
Wang, H., Hughes, R.E., Steele, J.D., Lepley, S.W., Tian, J., 2003. Correlation of climate cycles in middle Mississippi Valley loess and Greenland ice. Geology 31, 179–182.
Wang, H., Stumpf, A.J., Miao, X., Lowell, T.V., 2012. Atmospheric changes in North America during the last deglaciation from dune-wetland records in the Midwestern United States. Quat. Sci. Rev. 58, 124–134.
Wang, H., Stumpf, A.J., Miao, X., 2013. Reply to comments by Curry et al. (2013) on" Atmospheric changes in North America during the last deglaciation from dune-wetland records in the Midwestern United States". Quat. Sci. Rev. 80, 200–203.
Wassenburg, J.A., Dietrich, S., Fietzke, J., Fohlmeister, J., Jochum, K.P., Scholz, D., Richter, D.K., Sabaoui, A., Spotl, C., Lohmann, G., 2016. Reorganization of the North Atlantic Oscillation during early Holocene deglaciation. Nat. Geosci. 9, 602–605.
Winters, A.C., Martin, J.E., 2017. Diagnosis of a north American Polar-subtropical jet superposition employing piecewise potential vorticity inversion. Mon. Weather Rev. 145, 1853–1873.

Woollings, T., Hannachi, A., Hoskins, B., 2010. Variability of the North Atlantic eddy-driven jet stream. Quart. J. R. Meteorol. Soc. 136, 856–868.
Wunsch, C., 2006. Abrupt climate change: An alternative view. Quat. Res. 65, 191–203.
Xie, S.C., Evershed, R.P., Huang, X.Y., Zhu, Z.M., Pancost, R.D., Meyers, P.A., Gong, L.F., Hu, C.Y., Huang, J.H., Zhang, S.H., Gu, Y.S., Zhu, J.Y., 2013. Concordant monsoon-driven postglacial hydrological changes in peat and stalagmite records and their impacts on prehistoric culture in Central Chian. Geology 41, 827–830.
Xue, D.K., Zhang, Y.C., 2017. Concurrent variations in the location and intensity of the Asian winter jet streams and the possible mechanism. Clim. Dyn. 49, 37–52.
Yeh, D., Tao, S., Li, M., 1959. The abrupt change of circulation over the Northern Hemisphere during June and October. In: Atmosphere and the Sea in Motion. Rossby Memorial. Rockefeller Institute, New York, pp. 249–267.
Yuan, D., 2004. Timing, Duration, and Transitions of the last Interglacial Asian Monsoon. Science 304, 575–578.
Zhang, E.L., Zhao, C., Xue, B., Liu, Z.H., Yu, Z.C., Chen, R., Shen, J., 2017. Millennial-scale hydroclimate variations in southwest China linked to tropical Indian Ocean since the last Glacial Maximum. Geology 45, 435–438.
Zhang, H., Griffiths, M.L., Chiang, J.C., Kong, W., Wu, S., Atwood, A., Huang, J., Cheng, H., Ning, Y., Xie, S., 2018. East Asian hydroclimate modulated by the position of the westerlies during termination I. Science 362, 580–583.
Zhou, W.J., Zheng, Y.H., Meyers, P.A., Jull, T.J., Xie, S.C., 2010. Postglacial climate-change record in biomarker lipid compositions of the Hani peat sequence Northeastern China. Earth Planet Sci. Lett. 294, 37–46.